applied sciences

MDPI

Article

Seismic Capacity of R/C Buildings Retrofitted with a V-Bracing System Equipped with a Novel Laterally Layered Friction Damper

Bok-Gi Lee [1], Jin-Young Kim [2], Ju-Seong Jung [1] and Kang-Seok Lee [3,*]

[1] Innovative Durable Building and Infrastructure Research Center, Hanyang University, Ansan 15588, Gyeonggi-do, Republic of Korea; dlqhrrl15@naver.com (B.-G.L.); jjsshm@naver.com (J.-S.J.)
[2] Department of Architectural Engineering, Hanyang University, Seoul 04763, Republic of Korea; jykim@jteceng.com
[3] Department of Architectural Engineering & Smart City Engineering, Hanyang University, Ansan 15588, Gyeonggi-do, Republic of Korea
* Correspondence: ksleenist@hanyang.ac.kr

Abstract: This study proposed a novel V-bracing system equipped with a laterally layered friction damper (LLFD), which can supplement the shortcomings of conventional vibration control systems and is applicable to existing reinforced concrete (R/C) buildings. A material test was used to evaluate the material performance and energy dissipation capacity of this LLFD. Pseudo-dynamic testing was conducted on two-story frame specimens based on an existing R/C building with non-seismic details to verify the seismic retrofitting effects of applying the LLFD V-bracing system to existing R/C frames, i.e., the restoring force characteristics, energy dissipation capacity, and seismic response control capacity. Based on the results of the material and pseudo-dynamic tests, restoring characteristics were proposed for the non-linear dynamic analysis of a building (frame specimen) retrofitted with the LLFD V-bracing system. A non-linear dynamic analysis was conducted based on the proposed restoring force characteristics, and the results obtained were compared with the pseudo-dynamic test results. Finally, for evaluating the commercialization potential of the LLFD V-bracing system, a non-linear dynamic analysis was conducted on an existing R/C building with non-seismic details retrofitted with the system. The seismic retrofitting effect was verified by examining the seismic response load and displacement characteristics, energy dissipation capacity, and damper load and displacement response before and after seismic retrofitting. The study results showed that the R/C frame (building) with non-seismic details exhibited shear failure at a design basis earthquake scale of 200 cm/s^2; however, light seismic damage could be expected for a frame (building) retrofitted with the LLFD V-bracing system. At a maximum considered earthquake scale of 300 cm/s^2, insignificant seismic damage was also anticipated, thereby verifying the validity of the newly developed LLFD V-bracing system.

Keywords: reinforced concrete; laterally layered friction damper; V-bracing; seismic capacity; seismic retrofitting; pseudo-dynamic testing; non-linear dynamic analysis

Citation: Lee, B.-G.; Kim, J.-Y.; Jung, J.-S.; Lee, K.-S. Seismic Capacity of R/C Buildings Retrofitted with a V-Bracing System Equipped with a Novel Laterally Layered Friction Damper. *Appl. Sci.* **2023**, *13*, 13205. https://doi.org/10.3390/app132413205

Academic Editor: Dario De Domenico

Received: 20 October 2023
Revised: 25 November 2023
Accepted: 7 December 2023
Published: 12 December 2023

Correction Statement: This article has been republished with a minor change. The change does not affect the scientific content of the article and further details are available within the backmatter of the website version of this article.

1. Introduction

Concrete buildings exhibit early deterioration and significant damage in vulnerable parts under improper design, material, construction, use, and environmental conditions, negatively affecting the safety, durability, and functionality of the structures, thereby increasing the frequency of natural disasters and safety accidents as well as the damage scale. In particular, safety accidents involving concrete structures have rapidly increased of late, along with the damage scale, owing to serious problems associated with the safety of concrete structures as their performance and functions degrade. Their normal deterioration is accelerated by changes in the surrounding environment (e.g., climate change) and load

conditions (e.g., quality errors in the design and construction, expansion, and design modification). Therefore, the safety of a concrete structure must be regularly monitored to effectively utilize its functions during its service life. When damage occurs or is likely to occur, safety must be secured through repair and reinforcement.

Meanwhile, cases of seismic damage to various facilities, especially buildings, have rapidly increased owing to large earthquakes worldwide, including the 2023 Turkey-Syria and Marrakesh-Safi earthquakes. Large earthquakes have caused significant seismic damage in Japan, China, and Taiwan, which are close to the Korean Peninsula, thus confirming that Korea could also be directly or indirectly affected by earthquakes. In particular, the 2005 Fukuoka earthquake in Japan, the 2008 Sichuan earthquake in China, and the 2016 Kumamoto earthquake in Japan occurred on the Eurasian Plate, which contains the Korean Peninsula. Thus, large earthquakes are also likely to occur in Korea.

As shown in Table 1, the frequency of earthquakes in Korea is increasing. In particular, the 2016 Gyeongju earthquake and the 2017 Pohang earthquake, which had recorded values of M = 5.8 and M = 5.4, respectively, produced a serious crisis related to the seismic safety of buildings in Korea. They clearly showed that large earthquakes are highly likely to occur in Korea, possibly causing national disasters. During the 2016 Gyeongju earthquake, no significant seismic damage occurred to buildings except for the columns of some buildings close to the epicenter, including school facilities and houses. However, the 2017 Pohang earthquake caused serious damage to school facilities with non-seismic details, newly built pilotis, and apartments [1]. The shear failure of R/C columns with insufficient shear reinforcement has emerged as an important issue related to the measures against earthquakes in Korea, as shown in Figure 1 [1].

Table 1. List of past earthquakes in Korea based on data collected by the Korea Meteorological Administration [2].

Year	City and Region	Magnitude (M)
1978	Hongseong, Chungcheongnam-do	4.9
1994	Sinan, Jeollanam-do	4.9
2003	Baengnyeong Island, Incheon	5.0
2004	Uljin, Gyeongsangbuk-do	5.2
2013	Sinan, Jeollanam-do	4.9
2013	Baengnyeong Island, Incheon	4.9
2014	Taean, Chungcheongnam-do	5.1
2016	Gyeongju, Gyeongsangbuk-do	5.8
2017	Pohang, Gyeongsangbuk-do	5.4
2019	Miryang, Gyeongsangnam-do	3.5
2021	Sinan, Jeollanam-do	3.7
2022	Goesan, Chungcheongbuk-do	4.1

In Korea, seismic design standards were first established in 1988. At that time, seismic design conditions were considered for buildings with six or more stories or with a total floor area of 100,000 m^2 or higher. The application targets were expanded to buildings with three or more stories or 1000 m^2 or higher in 2005 and those with three or more stories or 500 m^2 or higher in 2015. The standards were strengthened to two or more stories or a total floor area of 500 m^2 or higher after the 2016 Gyeongju earthquake and have been implemented since February 2017. Considering the increasing magnitude and frequency of earthquakes in Korea, to minimize the human casualties and property damage caused by the collapse of buildings in the event of a large earthquake, it is important to develop economical and effective seismic retrofitting methods that can improve the seismic performances of buildings expected to be vulnerable to earthquakes, especially

R/C buildings with non-seismic details, which are expected to exhibit the shear failure of columns. Seismic retrofitting must be performed using an efficient and economical method according to the expected seismic magnitude and degree of damage.

Figure 1. Shear damage of R/C buildings in the 2017 Pohang Earthquake [1].

Typical seismic retrofitting methods for existing R/C buildings include using various reinforcing materials such as steel braces, precast concrete, and steel plates, as well as increasing the cross-sectional area through pouring. Representative types include the wall construction method, jacketing method, steel plate reinforcement method, and steel bracing seismic retrofitting [3–13]. However, all these seismic retrofitting methods have shortcomings [5,14,15], as listed below:

- They increase the weight of a building. Thus, buildings with weak foundations, such as R/C buildings with non-seismic details, may require foundation reinforcement.
- Securing a workspace is difficult during seismic retrofitting, and the utilization of space is limited.
- In the case of the steel plate reinforcement method (one of the most commonly used methods), the weight of the steel plate makes transport and pressing work difficult. In particular, when steel plate pressing is applied to a damaged structure, it is impossible to confirm whether the adhesion between the parent material and the steel plate is sufficient. In some cases, heavy steel plates hang from the parent material, causing further problems.
- Accurate construction is required.

To address the above problems, new retrofitting methods have been developed using new composite materials such as carbon, aramid, and glass fibers, and these have attracted attention [16–19]. However, these methods also have several shortcomings [15], as listed below:

- Preparation is required for rough surface work.
- The reinforcement effect varies depending on the fiber direction (i.e., the anisotropy problem).
- Securing a workspace is difficult when construction is performed in a narrow space.
- Expensive materials.
- Applying ductile reinforcement to non-seismic detailed buildings with insufficient shear strength is inefficient.

As described above, while the importance of seismic retrofitting has recently increased as one of the measures against earthquakes, conventional seismic retrofitting methods have many shortcomings when applied to buildings with non-seismic details, such as increased weight, problems with securing construction space, and economic feasibility problems.

In recent years, vibration control systems have been developed and utilized to secure seismic stability in buildings while considering technical and social demands. The ASCE 7-10 [20] and ASCE/SEI 7-22 [21] standards of the United States reflect the procedures for applying seismic design to vibration control systems, including dampers and seismic resistance systems. JBDPA [22] of Japan and KDS 41 [23] of Korea also include standards to allow vibration control system design, which includes seismic isolation and damping structures, to be reflected in structural design. However, considering conventional vibration control systems are typically installed at the building construction stage, they involve excessive costs when installed in existing buildings for seismic reinforcement because it is difficult to install them at a later stage; moreover, the reinforcement effect may not be satisfactory because of a vibration control system installation error for the expected level of the seismic load, and buckling may occur. It is also difficult to apply them for the seismic reinforcement of R/C buildings, which have a relatively small deformation capacity compared to steel frame buildings; in particular, they are prone to bending deformation under out-of-plane loads.

Therefore, these issues highlight the need to develop a new vibration control system that supplements and overcomes the above-mentioned shortcomings of conventional vibration control systems. Zhang et al. [24] developed superelastic shape memory alloy wire dampers and verified their performance through analytical studies, and Matteis et al. [25] performed FEA of metal shear panels and R/C structures to which metal shear panels were applied. Performance was verified through full-scale tests. Vemuri [26] conducted research on a link that acts as a sacrificial fuse by dissipating seismic energy among the key components of EBF. Shi et al. [27] verified the self-centering performance of buildings when analyzing the parameters of shape memory alloy braces and applying them, and Yao et al. [28] conducted an experimental analysis of low-yield-point steel shear panel dampers. Ferraioli et al. [29] conducted an analytical study on buildings using continuous energy-dissipative steel columns.

In addition, a variety of studies have been conducted on friction dampers rather than just metal dampers. Mualla et al. [30] presented a novel friction damper device and conducted research on the type and frequency influence of friction pads, and Monir et al. [31] performed experiments and analysis by applying the friction damper as diagonal bracing. Ghorbani et al. [32] proposed a friction damper with two slip loads and verified the seismic performance through nonlinear dynamic analysis. Veismoradi et al. [33] verified the performance of the self-centering rotational friction damper that can provide both energy dissipation as well as self-centering characteristics through experimentation and FEA. Qiu et al. [34] developed a self-centering damper that exploits the shape memory alloy bolts and variable friction mechanism and verified its performance through experiments and FEA.

This study proposed a novel V-bracing system equipped with a laterally layered friction damper (LLFD), which can supplement the shortcomings of conventional vibration control systems and is applicable to existing R/C buildings. The material performance and energy dissipation capacity of the LLFD were evaluated through a material test. In addition, pseudo-dynamic testing was conducted on two-story frame specimens based on an existing R/C building with non-seismic details to verify the seismic retrofitting effect of applying the LLFD V-bracing system to existing R/C frames, i.e., the restoring force characteristics, energy dissipation capacity, and seismic response control capacity. Based on the results of the material test and pseudo-dynamic test, restoring force characteristics were proposed for the non-linear dynamic analysis of a building (frame specimen) retrofitted with the LLFD V-bracing system. A non-linear dynamic analysis was conducted based on the proposed restoring force characteristics, and the results obtained were compared with the pseudo-dynamic test results.

Finally, for evaluating the commercialization potential of the LLFD V-bracing system, a non-linear dynamic analysis was conducted on the existing R/C building with non-seismic details retrofitted with the system. The seismic retrofitting effect was verified by examining

the seismic response load and displacement characteristics, energy dissipation capacity, and damper load and displacement response before and after seismic retrofitting.

2. Proposal and Overview of LLFD V-Bracing System

2.1. Problems with Conventional Friction Damper Seismic Retrofitting Methods

Friction dampers, i.e., one of the dampers used for vibration control, have been widely used because they are easy to produce and design, can secure both economic feasibility and structural safety, and efficiently absorb seismic input energy. However, existing friction dampers have low seismic energy dissipation capacities because they are produced as vertical dampers, thus making them prone to out-of-plane bending deformation and bucking in the axial direction under seismic loads. Thus, this study examined the seismic performance of an LLFD under out-of-plane loads by testing the existing typical vertical layer friction damper (VLFD) and the proposed LLFD. The LLFD was produced as a galvanized steel plate by applying zinc plating to SS275 steel. Based on the research results of Kulak et al. [35], the designed friction coefficient (μ) was equal to 0.18. As shown in Figure 2, a displacement of up to 10 mm by an out-of-plane load was applied before applying the in-plane load in the test. The in-plane load was applied 10 times for 11 mm, 5 times for 22 mm, and 3 times for 33 mm to examine the seismic performances of the VLFD and LLFD.

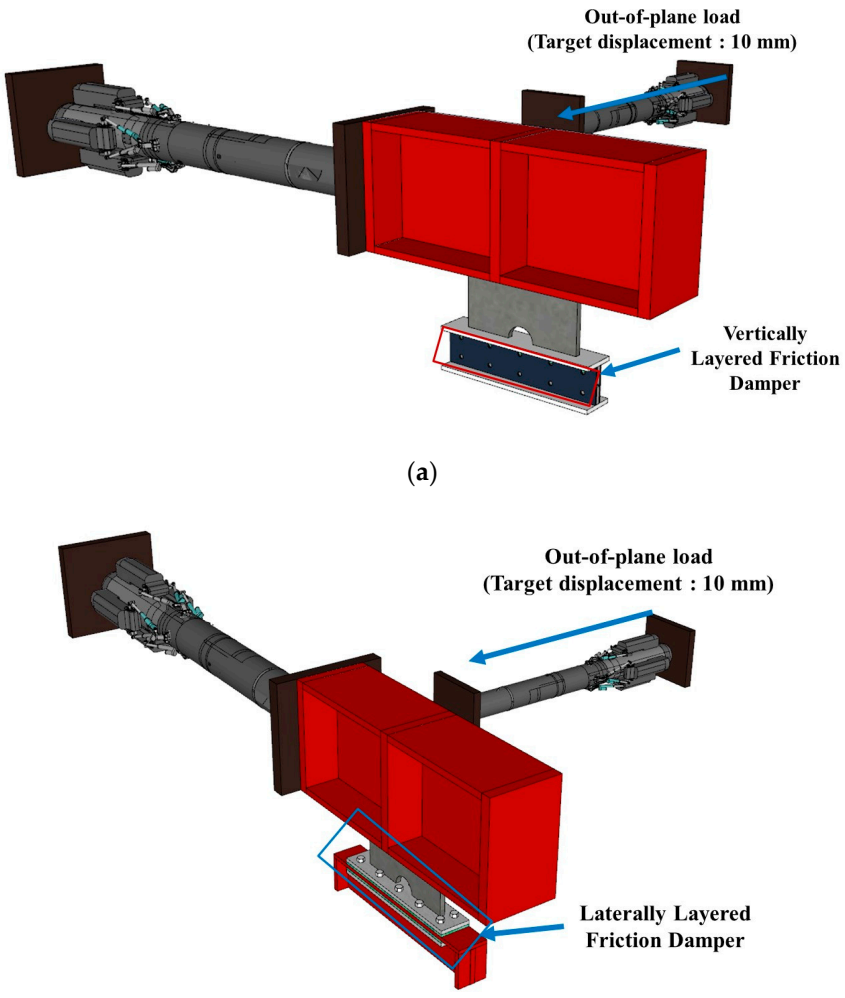

Figure 2. Set-up of VLFD and LLFD specimens for preliminary device test: (**a**) VLFD; (**b**) LLFD.

VLFD and LLFD specimens were designed using Equations (1) and (2), i.e., the design formulas for friction joints in the slip limit state from the steel structure design standards of KDS 41 [23], as listed in Table 2. Their design strength (yield strength) was 126.0 kN.

$$\varnothing R_n = \varnothing \cdot \mu \cdot h_f \cdot N_s \cdot N \cdot T_{volt} \quad (1)$$

$$T_{volt} = \frac{T_0}{kd_1} \quad (2)$$

Here, $\varnothing R_n$ is the design strength of the friction joints, $\varnothing$ is the shape reduction factor, μ is the friction coefficient, h_f is the filler coefficient, T_{volt} is the clamp force of the bolted joint, N_s is the number of shear surfaces, N is the number of bolts, T_0 is the torque, k is the torque coefficient, and d_1 is the diameter of the bolt.

Table 2. Design strength of VLFD and LLFD specimens used in the device test for preliminary investigation of their structural properties.

Specimens	Number of Shear Surface (N_s)	Number of Bolt (N)	Diameter of Bolt (d_1) [mm]	Torque (T_0) [N·m]	Clamp Force of Bolted Joint (T_{bolt}) [kN]	Design Strength of Friction Joints ($\varnothing R_n$) [kN]
VLFD	2	8	16	150	62.5	126.0
LLFD	2	8	16	150	62.53	126.0

$\varnothing$ = 0.7: Shape reduction factor, μ = 0.18: Friction coefficient [35], h_f = 1.0: Filler coefficient, k = 0.15: Torque coefficient.

Figure 3 shows the damage to the friction dampers after applying a target displacement of up to 10 mm to the out-of-plane load. The VLFD was damaged, but the proposed LLFD was not damaged despite the deformation of the H-frame. After applying the out-of-plane load, in-plane cyclic loading was applied. Figure 4 shows the load–displacement curves of the VLFD and LLFD for 11 mm (10 times), 22 mm (5 times), and 33 mm (3 times). A comparison of the curves showed that the VLFD had a value of 46.4 kN, i.e., approximately one-third of the design yield strength. In contrast, LLFD exhibited a value of 103.8 kN, slightly lower than the design strength, but exhibited a higher energy dissipation capacity than the existing horizontal friction damper because of its high strength.

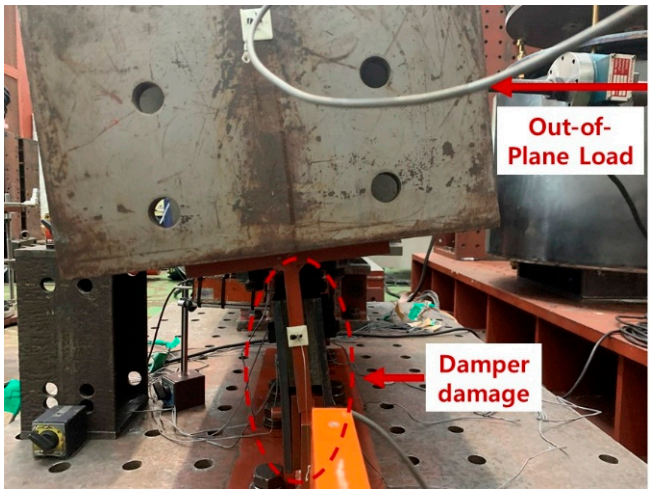

(**a**)

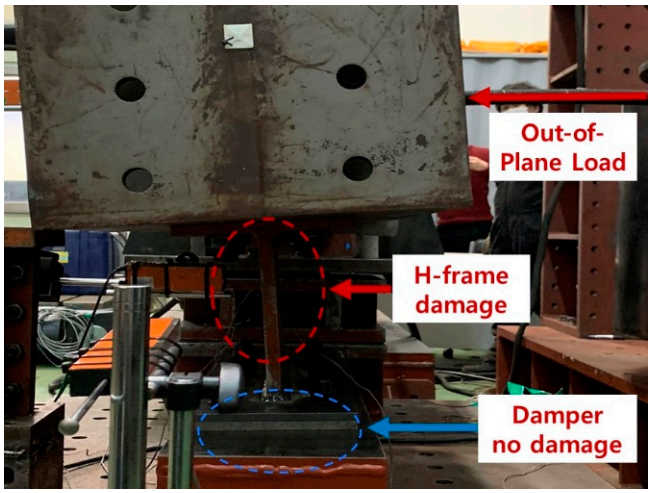

(**b**)

Figure 3. Damage of VLFD and LLFD specimens after out-of-plane load: (**a**) VLFD; (**b**) LLFD.

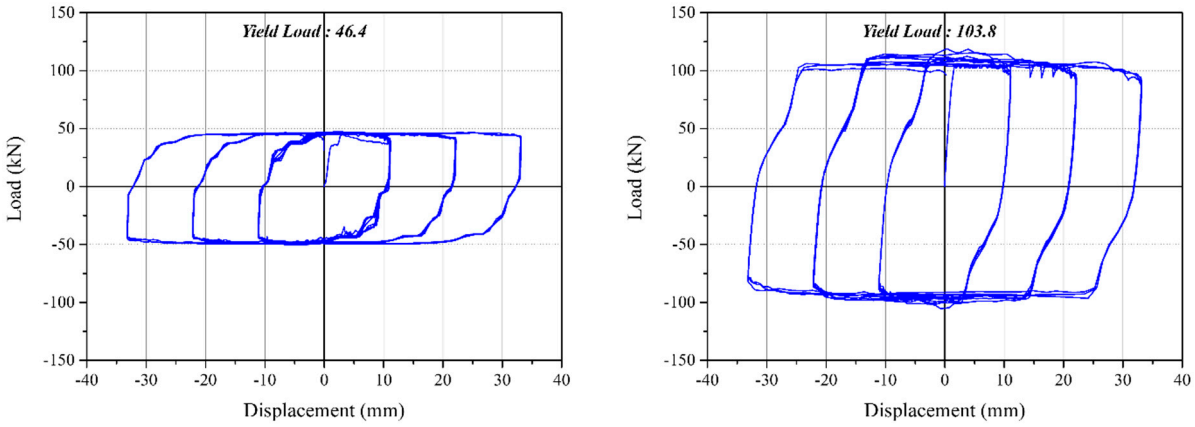

(**a**) (**b**)

Figure 4. Load−displacement relations of VLFD and LLFD specimens after final stage: (**a**) VLFD; (**b**) LLFD.

Based on the above results, this study developed an LLFD seismic retrofitting method that prevented damper deformation by out-of-plane loads and provided a stable energy dissipation capacity compared to the VLFD, thus confirming that the LLFD method could facilitate retrofitting design and secure both economic feasibility and seismic safety.

2.2. Components of the LLFD Method

Figure 5 shows the novel V-bracing system equipped with the LLFD proposed in this study. As shown in Figure 5b, the system can stably dissipate seismic energy through the strength of the friction damper in the event of an earthquake by installing the damper in a horizontal direction and preventing the bending and buckling caused by out-of-plane loads. The LLFD consists of the following: (a) steel bar, (b) connection plate, (c) damper plate, (d) nuts and bolts, (e) cover plate, (f) H-frame, and (g) the existing R/C member.

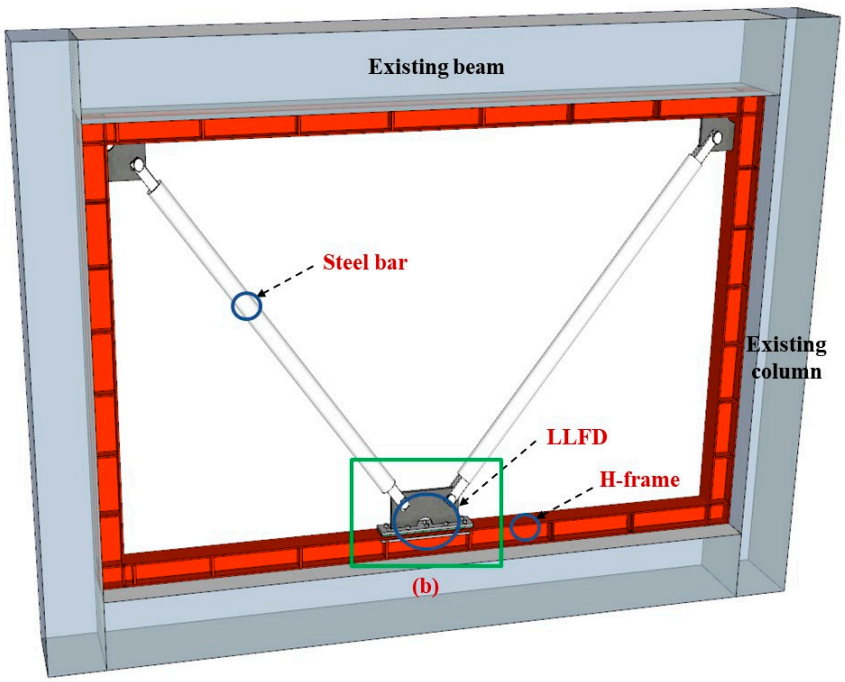

(**a**)

Figure 5. *Cont.*

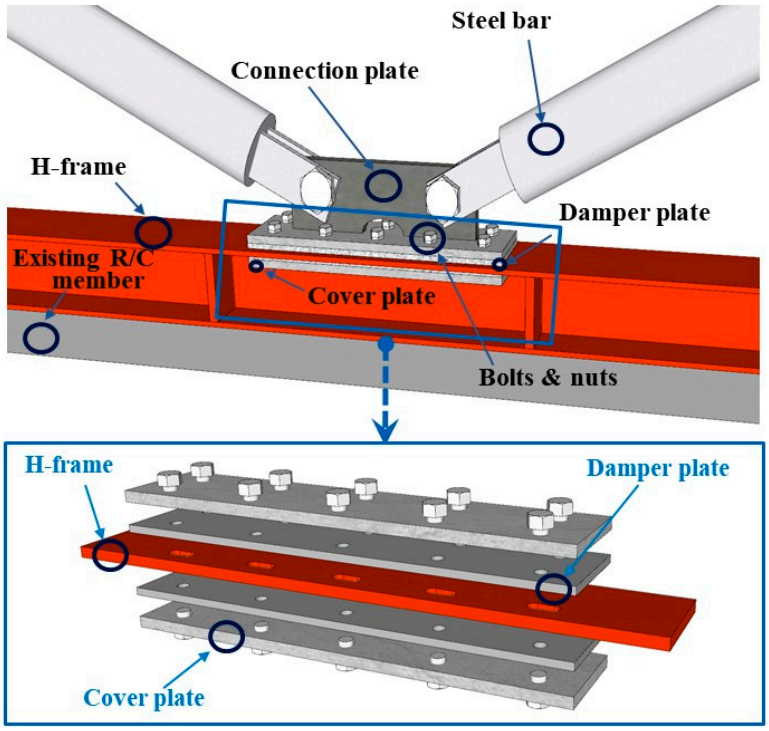

(**b**)

Figure 5. V-bracing seismic control system equipped with a novel laterally-layered friction damper: (**a**) V-Bracing System; (**b**) Details of LLFD.

The horizontal friction damper connects the steel bar and connection plate using hinges and combines the damper plate with the H-frame. The H-frame provides a stiffness reinforcement effect, while the damper plate provides a vibration control reinforcement effect. All these members can be installed using bolts without welding.

3. Material Test and Results for LLFD

3.1. LLFD Material Test Plan

In a friction damper, a friction force is generated in the sliding and opposite directions by the relative displacement between two materials in contact. This friction force releases the plastic deformation of the building through vibration in the form of thermal energy. Full-size specimens were prepared to verify the seismic performance of the developed LLFD, with a material test conducted using cyclic lateral loads based on the displacement required for the target performance. Meanwhile, the design strength of an LLFD for friction joints was calculated using Equations (1) and (2), i.e., the design formulas for the slip limit state in the steel structure design standards of KDS 41 [23]. Figure 6 shows the details of the LLFD used in the material test, while Table 3 lists the design strengths of friction joints calculated using the theoretical formulas.

As shown in Figure 6 and Table 3, two types of friction dampers, which employed widely used friction pads and galvanized plates, were used in the LLFD material test. The test was conducted by preparing two specimens for each friction damper. A friction pad (FP) was applied to the FP-LLFD specimen, which had a width of 600 mm, a height of 170 mm, and a thickness of 10 mm. The bolts used were D16-8EA, and the designed friction coefficient (μ = 0.2) was based on the research result [35]. The galvanized steel plate (GS)-LLFD specimen, with its geometry and number of bolts the same as those of the FP-LLFD, was produced by applying zinc plating to SS275. The designed friction coefficient (μ) had a value of 0.18.

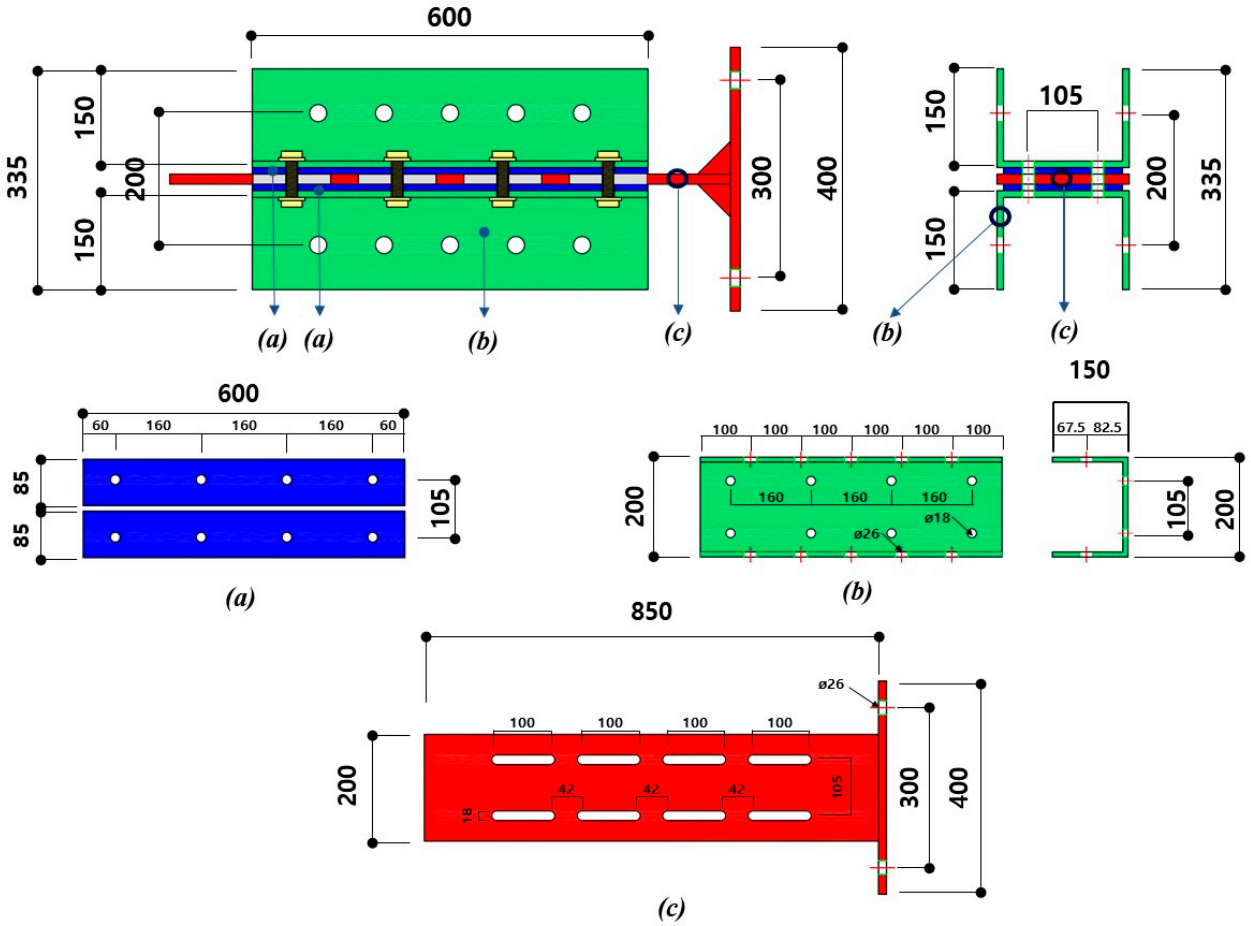

Figure 6. Details of LLFD used in device test (Unit: mm).

Table 3. Specimens of the LLFD used in the device test and calculation results.

Specimens	Number of Shear Surface (N_s)	Number of Bolt (N)	Diameter of Bolt (d_1) [mm]	Torque (T_0) [N·m]	Clamp Force of Bolted Joint (T_{bolt}) [kN]	Design Strength of Friction Joints ($\varnothing R_n$) [kN]
FP-LLFD-1 FP-LLFD-2	2	8	16	100	41.6	93.3
				200	83.3	186.6
				300	125	280.0
GS-LLFD-1 GS-LLFD-2	2	8	16	100	41.6	84.0
				200	83.3	168.0
				300	125	252.0

FP indicates Friction pad. GS indicates Galvanized steel plate. $\varnothing = 0.7$: Shape reduction factor depending on slot shapes, μ: Friction coefficient, $\mu = 0.2$ for FP-LLFD and $\mu = 0.18$ for GS-LLFD [35], $h_f = 1.0$: Filler coefficient, $k = 0.15$: Torque coefficient.

3.2. LLFD Material Test Loading and Measurement Methods

Figure 7 shows the installation of the LLFD specimens and the details of the measuring instruments. The horizontal load was applied by controlling the displacement using a 500-kN actuator. Linear variable differential transformers (LVDTs) were installed on each specimen to measure the displacement and base slip of the friction damper. The loading was applied to the LLFD specimens based on the measured displacement of the vibration control system, [LVDT (1) + LVDT (2)]/2.

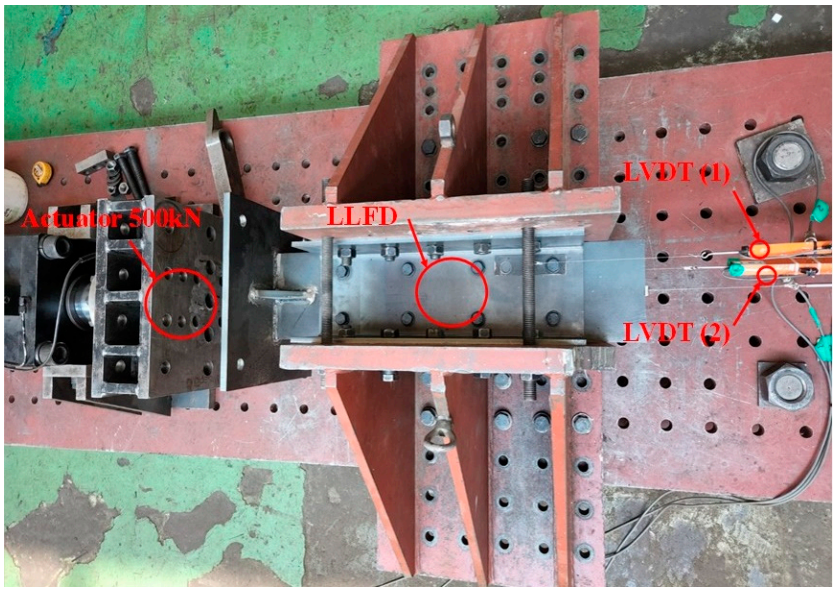

Figure 7. Specimen installation and measurement device (Top view).

The loading point of the actuator was matched to the center of the hardware for loading at the top of the specimen, with cyclic loading applied 10 times at 0.33 times the system displacement expected under the maximum considered earthquake (MCE), 5 times at 0.67 times this displacement, and 3 times at 1.0 times this displacement, based on the results of the 17.6 prototype test from the Korean seismic design standard [23] (see Figure 8). An allowable story drift of 1% (33 mm) for school buildings (special grade), which were the target buildings, was set as the maximum displacement expected under the MCE [23].

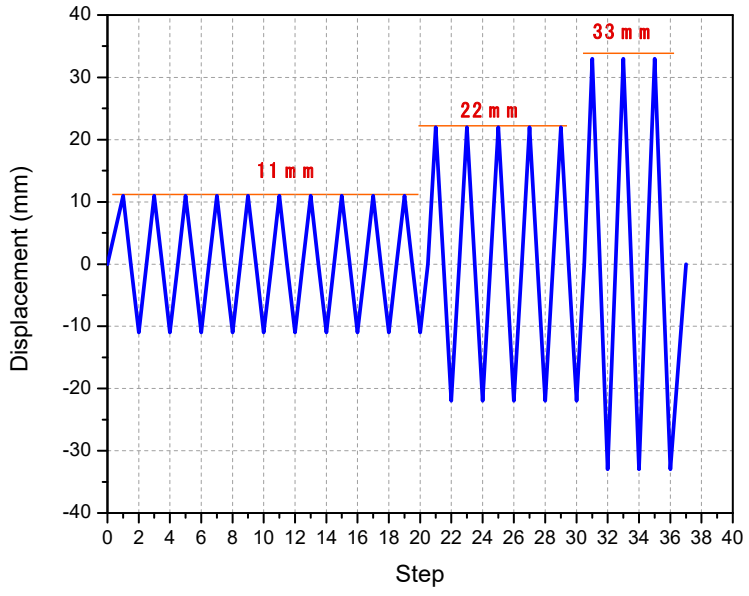

Figure 8. Repeated loading plan.

3.3. LLFD Material Test Results and Analysis

3.3.1. Comparison and Analysis of Load–Displacement Curves

Figure 9 shows the situations for the FP-LLFD and GS-LLFD specimens at a final control displacement of 33 mm. Figure 10 compares the load–displacement curves of the specimens under a torque pressure of 100–300 N-m, while Table 4 lists the yield displacements and yield loads of the specimens.

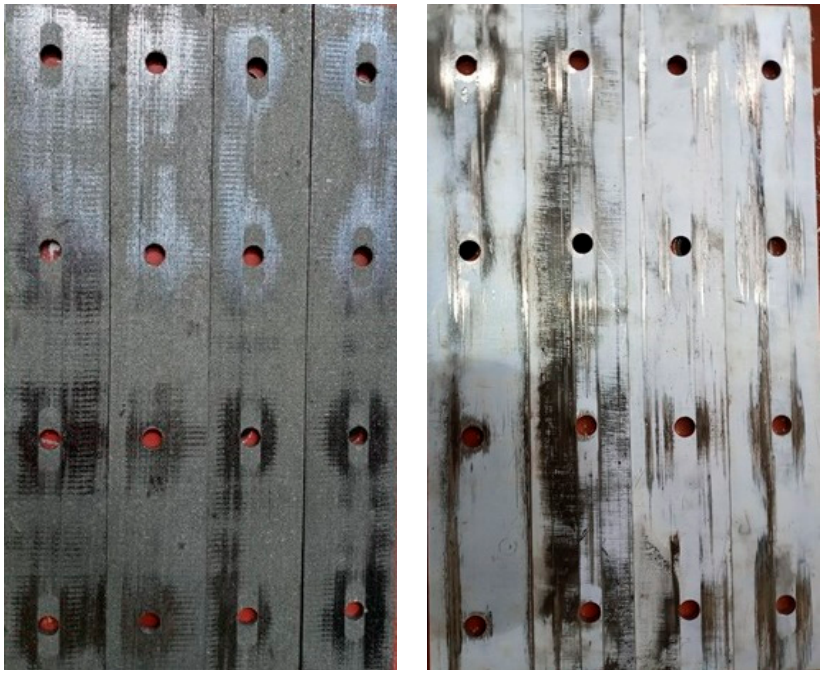

(**a**) (**b**)

Figure 9. Specimens at final control displacement of 33 mm: (**a**) FP-LLFD; (**b**) GS-LLFD.

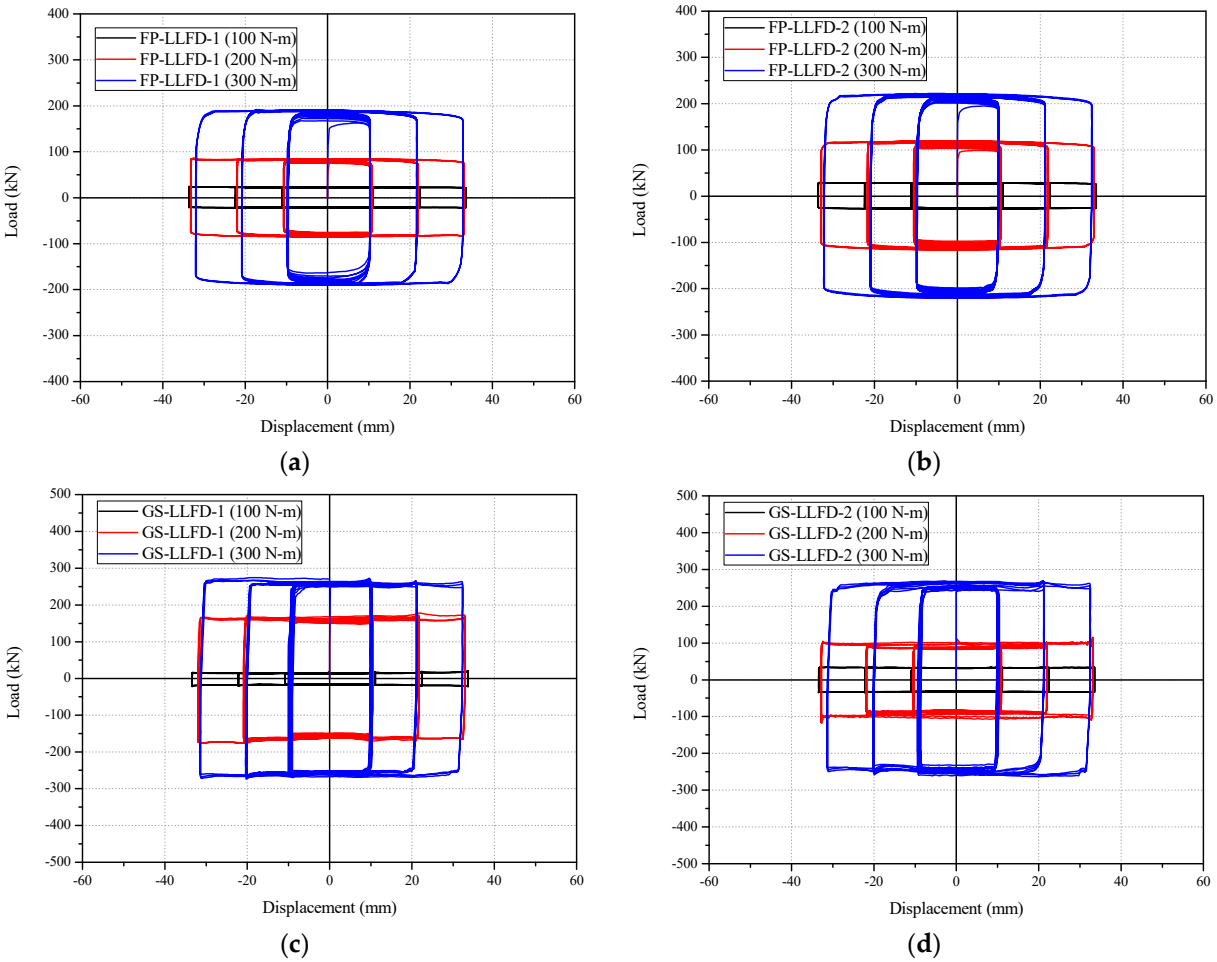

Figure 10. Load–displacement curve: (**a**) FP-LLFD-1; (**b**) FP-LLFD-2: (**c**) GS-LLFD-1; (**d**) GS-LLFD-2.

Table 4. Test results for NBSD specimens for FP-LLFD and GS-LLFD.

Specimens	Torque (N·m)	Yield State		Maximum Strength	
		Displacement $\delta_{d,y}$ (mm)	Strength $V_{d,y}$ (kN)	Positive $V_{d,max}$ (kN)	Negative $V_{d,min}$ (kN)
FP-LLFD-1	100	0.11	22.6	24.7	23.0
	200	0.41	76.1	86.8	85.0
	300	0.41	151.0	192.0	190.3
FP-LLFD-2	100	0.04	23.4	29.8	27.0
	200	0.11	81.2	119.6	116.0
	300	0.08	159.8	221.8	220.7
GS-LLFD-1	100	0.04	20.2	21.3	22.6
	200	0.08	145.0	177.7	176.3
	300	0.18	252.2	274.2	273.8
GS-LLFD-2	100	0.36	33.2	34.8	34.9
	200	0.17	111.7	114.9	118.0
	300	0.39	238.7	269.7	263.4

The FP-LLFD-1 specimen exhibited yield displacements and yield strengths of 0.11 mm and 22.6 kN under 100 N-m torque, 0.41 mm and 76.1 kN under 200 N-m torque, and 0.41 mm and 151.0 kN under 300 N-m torque, respectively. The FP-LLFD-2 specimen showed yield displacements and yield strengths of 0.04 mm and 23.4 kN under 100 N-m torque, 0.11 mm and 81.2 kN under 200 N-m torque, and 0.08 mm and 159.8 kN under 300 N-m torque, respectively.

The GS-LLFD-1 specimen showed yield displacements and yield strengths of 0.04 mm and 20.2 kN under 100 N-m torque, 0.08 mm and 145.0 kN under 200 N-m torque, and 0.18 mm and 252.2 kN under 300 N-m torque, respectively. The GS-LLFD-2 specimen exhibited yield displacements and yield strengths of 0.36 mm and 33.2 kN under 100 N-m torque, 0.17 mm and 111.7 kN under 200 N-m torque, and 0.39 mm and 238.7 kN under 300 N-m torque, respectively. Figure 11 shows the relationships between the torque pressure and yield strength for the FP-LLFD and GS-LLFD specimens. The figure shows the theoretical design strengths calculated by Equation (1) and an approximation equation based on regression analysis for comparison with the test results.

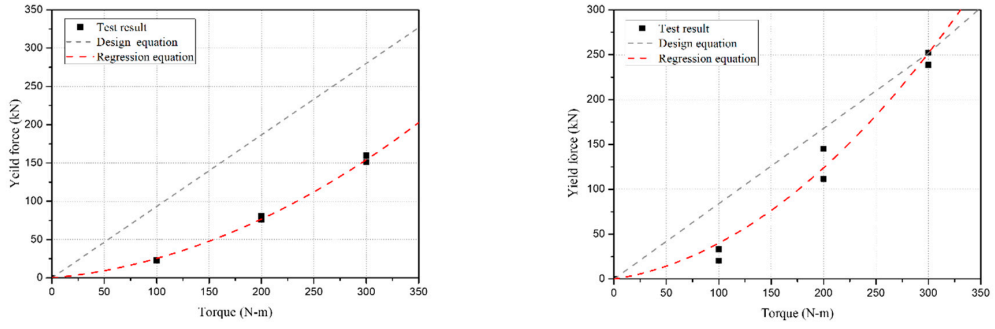

(**a**) (**b**)

Figure 11. Relationships between torque and yield force: (**a**) FP-LLFD; (**b**) GS-LLFD.

Overall, the test results for the FP-LLFD and GS-LLFD in the 100–300 N·m torque range were approximately twice as low as the design strength. Therefore, the non-linear dynamic analysis of two-story R/C frames with LLFDs described in Sections 5 and 6, as well as a non-linear dynamic analysis of the entire building for seismic retrofitting design

using LLFDs, were conducted using regression Equations (3) and (4) because the LLFD theoretical design formula presented by Equation (1) had a large error. The coefficients of determination (R2) of Equations (3) and (4) had values of 0.99 and 0.98 for the FP-LLFD and GS-LLFD specimens, respectively, indicating very high correlations.

$$V_{d,y} = 0.0013 \cdot T_0^2 + 0.124 T_0 \text{ (forFP-LLFD)} \quad (3)$$

$$V_{d,y} = 0.0022 \cdot T_0^2 + 0.184 T_0 \text{ (forGS-LLFD)} \quad (4)$$

3.3.2. Performance Compatibility Conditions of LLFD

As previously mentioned, a cyclic loading test was conducted based on the test method for displacement-dependent vibration control devices presented in KDS 41 [23] as a test for damping systems. The performance compatibility of the vibration control system was evaluated based on the test results and the KDS 41 [23] standard shown in Table 5. Tables 6–9 show the results of evaluating the performance compatibilities of the proposed FL-LLFD-1, FL-LLFD-2, GS-LLFD-1, and GS-LLFD-2 specimens. The suitability of each specimen was evaluated based on a maximum displacement of 33 mm, with the results indicating that all the LLFD specimens exhibited suitable performances as displacement-dependent vibration control devices.

Table 5. Performance suitability conditions of displacement-dependent seismic control device [23].

Criterion	Performance Requirements
1	During cyclic loading for a certain number of cycles, both the maximum load ($V_{d,max}$) and the minimum load ($V_{d,min}$) measured at the zero-displacement point are required to be within 15% of the average ($V_{d,ave}$) of all measured loads.
2	During cyclic loading for a certain number of cycles, the loads measured in each direction at the maximum device displacement are required to be within 15% of the average of all measured loads.
3	During cyclic loading for a certain number of cycles, the area of the hysteresis loop measured by RCom the damper (E_d) is required to be within 15% of the average of all measured hysteresis loop areas ($E_{d,ave}$).

Table 6. Performance suitability evaluation of seismic control device of FL-LLFD-1 specimen.

Classification	Performance Suitability Conditions				
Condition 1	Cycle	1	2	3	Average
	$V_{d,max}$ (kN)	190.3	190.3	184.5	188.4
	$V_{d,min}$ (kN)	−188.7	−189	−190	−189.2
	$(V_{d,max} - V_{ave})/V_{ave}$	1.01	1.01	−2.07	-
	$(V_{d,min} - V_{ave})/V_{ave}$	−0.26	−0.11	0.42	-
	Result	Conforming	Conforming	Conforming	-
Condition 2	Cycle	1	2	3	Average
	$V_{d,max}$ (kN)	171.3	170.5	169.4	170.4
	$V_{d,min}$ (kN)	−173.6	−173.1	−173.5	−173.4
	$(V_{d,max} - V_{ave})/V_{ave}$	0.53	0.06	−0.59	-
	$(V_{d,min} - V_{ave})/V_{ave}$	0.12	−0.17	0.06	-
	Result	Conforming	Conforming	Conforming	-
Condition 3	Cycle	1	2	3	Average
	E_d (kN·mm)	23.4	22.8	23.2	23.1
	$(E_d - E_{d,ave})/E_{d,ave}$	1.3	−1.3	0.43	-
	Result	Conforming	Conforming	Conforming	-

Table 7. Performance suitability evaluation of seismic control device of FL-LLFD-2 specimen.

Classification	Performance Suitability Conditions				
Condition 1	Cycle	1	2	3	Average
	$V_{d,max}$ (kN)	220.4	221.5	218.6	220.2
	$V_{d,min}$ (kN)	−219.3	−220.3	−220.6	−220.1
	$(V_{d,max} - V_{ave})/V_{ave}$	0.09	0.59	−0.73	-
	$(V_{d,min} - V_{ave})/V_{ave}$	−0.36	0.09	0.23	-
	Result	Conforming	Conforming	Conforming	-
Condition 2	Cycle	1	2	3	Average
	$V_{d,max}$ (kN)	196.3	199.1	199.2	198.2
	$V_{d,min}$ (kN)	−192.9	−199.3	−200.3	−197.5
	$(V_{d,max} - V_{ave})/V_{ave}$	−0.96	0.45	0.5	-
	$(V_{d,min} - V_{ave})/V_{ave}$	−2.33	0.91	1.42	-
	Result	Conforming	Conforming	Conforming	-
Condition 3	Cycle	1	2	3	Average
	E_d (kN·mm)	27.4	27.8	27.2	27.5
	$(E_d - E_{d,ave})/E_{d,ave}$	−0.36	1.09	−1.09	-
	Result	Conforming	Conforming	Conforming	-

Table 8. Performance suitability evaluation of seismic control device of GS-LLFD-1 specimen.

Classification	Performance Suitability Conditions				
Condition 1	Cycle	1	2	3	Average
	$V_{d,max}$ (kN)	259.7	259	260.8	259.8
	$V_{d,min}$ (kN)	−262.7	−261.3	−267	−263.7
	$(V_{d,max} - V_{ave})/V_{ave}$	−0.04	−0.31	0.38	-
	$(V_{d,min} - V_{ave})/V_{ave}$	−0.38	−0.91	1.25	-
	Result	Conforming	Conforming	Conforming	-
Condition 2	Cycle	1	2	3	Average
	$V_{d,max}$ (kN)	247.8	256.4	263.6	255.9
	$V_{d,min}$ (kN)	−258.7	−266	−271.9	−265.5
	$(V_{d,max} - V_{ave})/V_{ave}$	−3.17	0.2	3.01	-
	$(V_{d,min} - V_{ave})/V_{ave}$	−2.56	0.19	2.41	-
	Result	Conforming	Conforming	Conforming	-
Condition 3	Cycle	1	2	3	Average
	E_d (kN·mm)	27.4	27.8	27.2	27.5
	$(E_d - E_{d,ave})/E_{d,ave}$	−0.36	1.09	−1.09	-
	Result	Conforming	Conforming	Conforming	-

Table 9. Performance suitability evaluation of seismic control device of GS-LLFD-2 specimen.

Classification	Performance Suitability Conditions				
Condition 1	Cycle	1	2	3	Average
	$V_{d,max}$ (kN)	262.8	267.9	267.7	266.1
	$V_{d,min}$ (kN)	−252.4	−253	−254	−253.1
	$(V_{d,max} - V_{ave})/V_{ave}$	−1.24	0.68	0.6	-
	$(V_{d,min} - V_{ave})/V_{ave}$	−0.28	−0.04	0.36	-
	Result	Conforming	Conforming	Conforming	-
Condition 2	Cycle	1	2	3	Average
	$V_{d,max}$ (kN)	246.6	255.1	260.4	254
	$V_{d,min}$ (kN)	−238.1	−244.7	−249	−243.9
	$(V_{d,max} - V_{ave})/V_{ave}$	−2.91	0.43	2.52	-
	$(V_{d,min} - V_{ave})/V_{ave}$	−2.38	0.33	2.09	-
	Result	Conforming	Conforming	Conforming	-
Condition 3	Cycle	1	2	3	Average
	E_d (kN·mm)	32.1	32	32.2	32.1
	$(E_d - E_{d,ave})/E_{d,ave}$	0	−0.31	0.31	-
	Result	Conforming	Conforming	Conforming	-

4. Pseudo-Dynamic Test Overview and Result Analysis

As shown in Figure 12, pseudo-dynamic tests were conducted on two-story frame specimens based on existing R/C school buildings with non-seismic details using the pseudo-dynamic test system constructed in this study to verify the seismic retrofitting effects of applying the developed LLFD V-bracing system to existing R/C buildings, i.e., the restoring force characteristics, energy dissipation capacity, and seismic response control capacity.

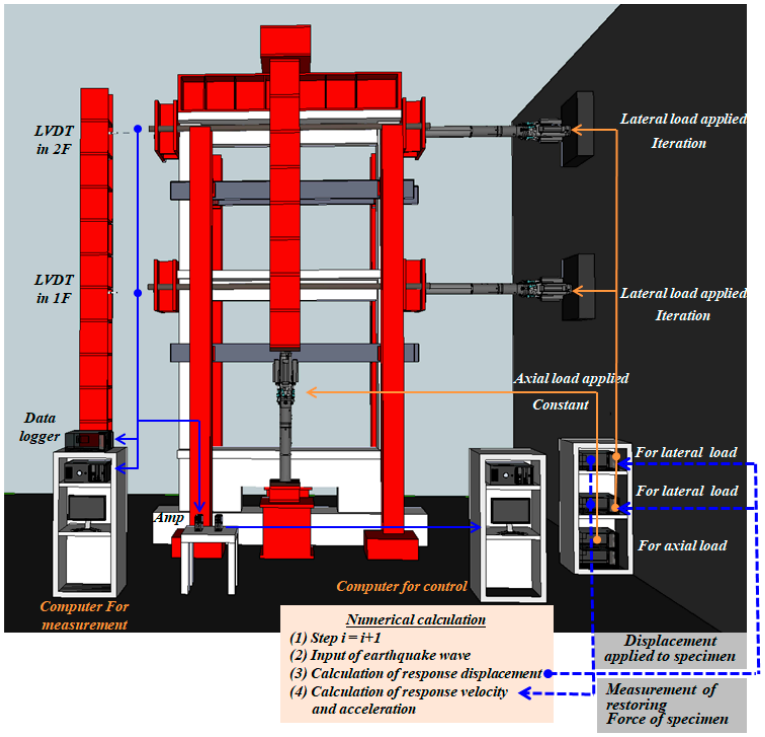

Figure 12. Proposed pseudo-dynamic testing system.

4.1. Overview of the Existing Seismic Test Method

In the event of an earthquake, its influence on a structure depends on the characteristics of the ground acceleration as well as the type, weight, and stiffness of the structure. The shear force in the vertical members that support the building caused by the horizontal seismic acceleration generates relative lateral motion in the building. In general, in the event of an earthquake, structures should withstand large deformations without collapse and absorb energy through inelastic behavior. In other words, while seismic loads are transmitted to a structure in the event of an earthquake, considerable seismic input energy is absorbed by the inelastic behavior of the structure because materials locally reach yield points and plastic deformation occurs in the structural system. However, it is extremely difficult or impossible to evaluate such inelastic behavior using theoretical methods, despite the development of computer software.

The experimental methods generally used to predict the inelastic seismic responses of structures can be classified into shaking-table, quasi-static, and pseudo-dynamic tests. A shaking-table test is the most effective for examining the seismic behavior of a structure. However, scale models are mostly used because the weight and size of specimens are significantly limited by the size and capacity of the shaking table, which causes a similarity problem with the actual structure. Due to these constraints, a quasi-static test that controls the displacement or load of the structure has commonly been used to evaluate the inelastic behavior of a real-size structure.

The pseudo-dynamic test, which combines the benefits of the shaking and quasi-static tests [36], is a composite experimental method that combines an experiment with numerical analysis. The pseudo-dynamic test consists of a numerical calculation by a computer and an experiment in which the specimen is loaded. In the numerical calculation, the equation of motion is calculated using numerical integration based on the response of the specimen to specific deformation, the input seismic acceleration, and the response of the current step measured in the experiment. In addition, the response deformation for the next step is calculated. In the loading experiment, the response deformation is applied to the specimen using loading devices such as actuators, and the resulting displacement history is measured. By repeating the above manipulations, the seismic response of the target structure is calculated, while a response deformation similar to that in the event of an earthquake is applied to the specimen, with the seismic response calculated using a computer.

The pseudo-dynamic test is similar to the quasi-static test except that the displacement to be applied to the structure is determined by numerical analysis during the test. In general, it is necessary to assume hysteretic characteristics when predicting the seismic response using numerical dynamic analysis. However, the pseudo-dynamic test can obtain an effect similar to the actual seismic response by directly measuring such information from the specimen, and it is used in several studies to evaluate the seismic performance of buildings [37–40].

4.2. Pseudo-Dynamic Test System and Method

Figure 12 shows the concept of the pseudo-dynamic test system constructed in this study, as well as the specimen setting. As shown in the figure, the system can be expressed in two degrees of freedom (TDF), and it consists of a numerical calculation based on the ground motion input by the control computer and an experiment in which the specimen is loaded. During the test, the calculated displacement response is applied to the specimen using two hydraulic actuators installed in the horizontal direction. The actual restoring force is physically measured during the test and then used in the control computer to calculate the displacement response. Data conversion is performed using an analog-to-digital/digital-to-analog converter (DA-16A, Tokyo Soki Kenkyujo Company [41]. In the pseudo-dynamic test, the seismic response is calculated by a closed-loop control system.

MTS's Pseudodynamic Testing Program [42] was used in the numerical calculation by the control computer. In the experiment, the response of the next step was calculated

using numerical integration and the equation of motion shown in Equation (5) based on the restoring force of the specimen after deformation, the input seismic acceleration, and the response of the current step measured using LVDTs.

$$M\ddot{y}(t) + C\dot{y}(t) + r(t)[= Ky(t)] = -M\ddot{y}_0 \tag{5}$$

Here, M, C, and K represent the mass, damping, and stiffness matrix of the structure, respectively; y is the relative displacement vector of each layer mass for the foundation; r is the restoring force vector; $\ddot{y}_0$ is the input ground acceleration.

The α-method [43] was used for the numerical integration of the equation of motion. The algorithm for the numerical integration of the pseudo-dynamic test is given by Equation (6), as follows:

$$Ma_{i+1} + (1+\alpha)Cv_{i+1} - \alpha Cv_i + (1+\alpha) - \alpha r_i = (1+\alpha)f_{i+1} - \alpha f_i \tag{6}$$

$$y_{i+1} = y_i + \Delta t v_i + \Delta t^2 \left[\left(\frac{1}{2} - \beta \right) a_i + \beta a_{i+1} \right] \tag{7}$$

$$v_{i+1} = v_i + \Delta t[(1-\gamma)a_i + \gamma a_{i+1}] \tag{8}$$

Here, y_i, v_i, and a_i are the nodal displacement, velocity, and acceleration at the same time as $i\Delta t$, respectively; Δt is the integral time interval; r_i is the restoring force vector at the node; f_i is the external load vector $(-M\ddot{y}_0)$.

For elastic structures, $r_i = Ky_i$ (K: the elastic stiffness matrix of the structure) holds. Here, α, β, and γ are variables used to control the numerical characteristics of the algorithm, where $-5 \leq \alpha \leq 0$, $\beta = \frac{(1-\alpha)^2}{4}$, and $\gamma = \frac{1}{2} - \alpha$ indicate unconditional stability.

The displacement response in the next step was calculated using Equations (5)–(8) based on the stiffness (K), mass (M), and stiffness proportional damping coefficient I of the structure. The damping factor was assumed to be 0.03, i.e., 3% of critical damping. The horizontal seismic response deformation was applied to the specimen using a 2000 kN hydraulic MTS actuator on the first and second floors, as shown in Figure 12. The horizontal displacement used for the displacement response calculation was measured using 300-mm LVDTs installed on each floor. As for the axial force, the axial load applied to the actual existing frame was distributed, with the load applied to each column using 1000-kN oil jacks installed on both sides of the specimen. Hachinohe (EW) [44], which exhibited the largest seismic response displacement among the seismic response displacement characteristics (ductility ratio) of existing historical seismic waves, was selected for the ground motion. The test was conducted using the pseudo-dynamic test system with acceleration magnitudes of 200, 300, 400, and 500 cm/s^2. Figure 13 shows time history records of the normalized ground motion accelerations used in the pseudo-dynamic test, respectively, together with their acceleration response spectrum.

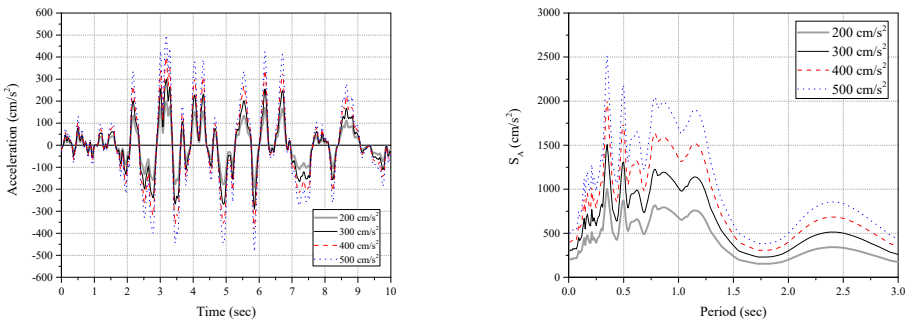

(**a**) (**b**)

Figure 13. Ground motion accelerations used in the pseudo-dynamic test. (**a**) Time history records and (**b**) acceleration response spectrum.

4.3. Materials Used and Their Characteristics

The concrete compressive strength of the specimens used in the pseudo-dynamic test was designed to be 21 MPa. The standard specimen correction value based on the average value of the three specimens was 97% of the measured compressive strength. The average compressive strength at 28 days was 21.4 MPa. The grade of the reinforcing bars used was SD400. D19 and D16 reinforcing bars were used as the main reinforcements for the columns, while D10 bars were used for shear reinforcements. Three tensile specimens were prepared for each reinforcing bar in accordance with KS B 0801 [45] to investigate the material properties of the reinforcing bars, with the tensile test conducted at a loading rate of 5 mm/min using a universal testing machine (UTM) in accordance with KS B 0802 [46]. In the test results, the average yield and tensile strengths were found to be 491 and 731 MPa for the D19 and D16 bars and 477 and 711 MPa for the D10 bars, respectively.

4.4. Specimen Preparation and Variables

The frame of an existing three-story R/C school building in Korea with non-seismic details (standard drawing type C in the 1980s) was selected, as shown in Figure 14, to examine the seismic performance of the LLFD method. The floor height of the building was 3.3 m, and the design strength of the concrete was 21 MPa. The target of the pseudo-dynamic test was the one-span, two-story real-size frame for the exterior of the school building. T-shaped beams were used for each floor, considering the effective slab width based on KDS 41 [23].

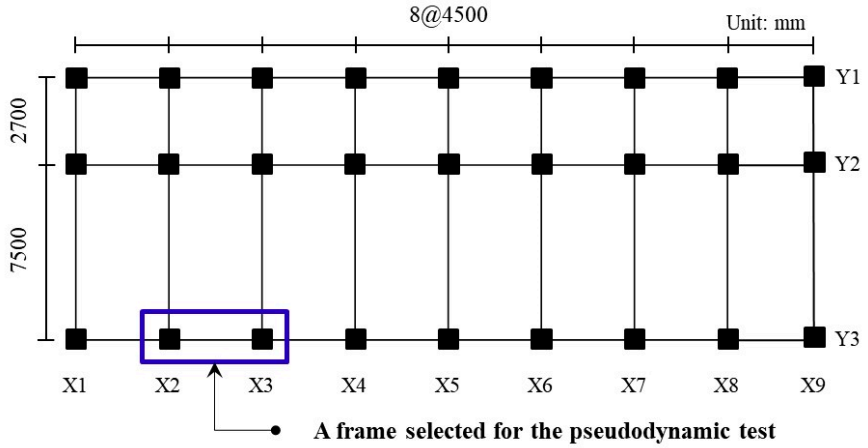

(**a**)

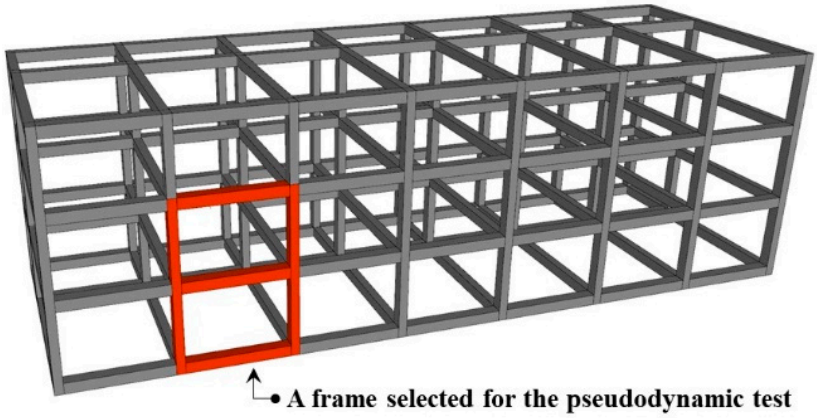

(**b**)

Figure 14. Selected R/C building and frame for the pseudo-dynamic testing: (**a**) planar view; (**b**) isometric view.

Figure 15 shows the reinforcement details for the existing frame and a photograph of the specimen. The pseudo-dynamic test was conducted by preparing two frame specimens as shown in Figure 16, including one frame specimen retrofitted with the LLFD V-bracing system and one non-reinforced frame specimen for a comparison with the LLFD-reinforced frame. In the test, the GS-LLFD was used based on the purchase conditions and economic characteristics. The GS-LLFD torque pressure was $T_0 = 200$ kN·m. In this instance, the yield strength was found to be 125 kN using regression Equation (4) in a member test.

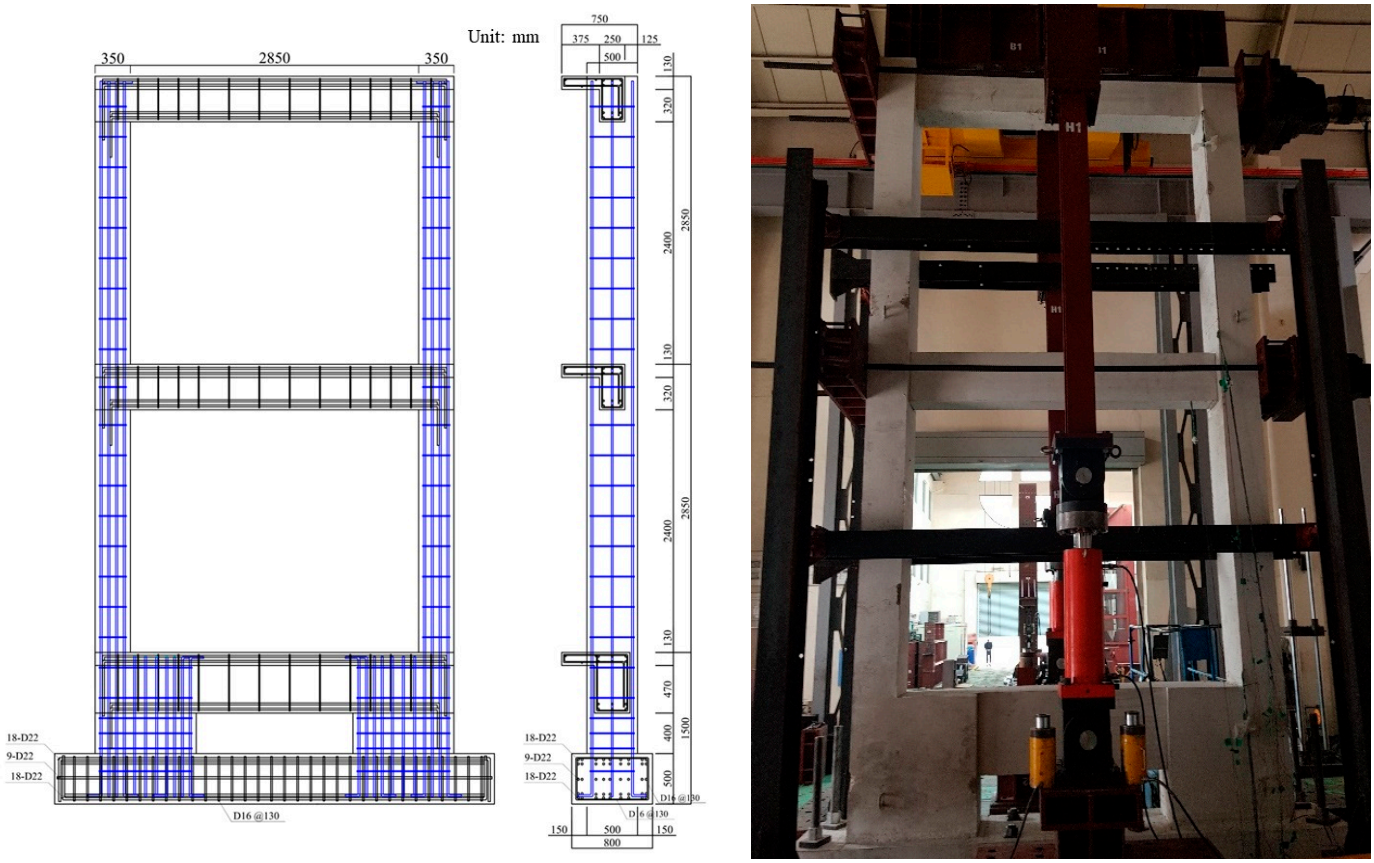

Figure 15. Detailed configuration of the control specimen (PD-RC): (**a**) specimen details; (**b**) photograph.

Hachinohe (EW), which exhibited the largest seismic response displacement, was selected as the input ground motion for the pseudo-dynamic test based on the results of research by Lee [44] on the seismic response displacement characteristics (ductility ratio) of medium- and low-rise R/C buildings (strength was less than 0.5 in the form of the shear force coefficient) during ten historical seismic waves. In the case of the seismic input acceleration, the Hachinohe (EW) seismic wave was standardized to sizes of 200, 300, 400, and 500 cm/s^2. The 200 and 300 cm/s^2 seismic scales corresponded to seismic zone-1 and ground types S_4 and S_5 at the level of two-thirds of the 2400-year return period earthquake specified in KDS 41 [23]. The 400 and 500 cm/s^2 seismic scales were used to examine the seismic retrofitting effect of the proposed LLFD V-bracing system in the event of a large earthquake, and they corresponded to the 2400-year return period earthquake. The axial load applied to the actual existing frame (two columns), i.e., 100 tons, was distributed, and an axial load of 50 tons was applied to each column. Table 10 lists the variables of the specimens.

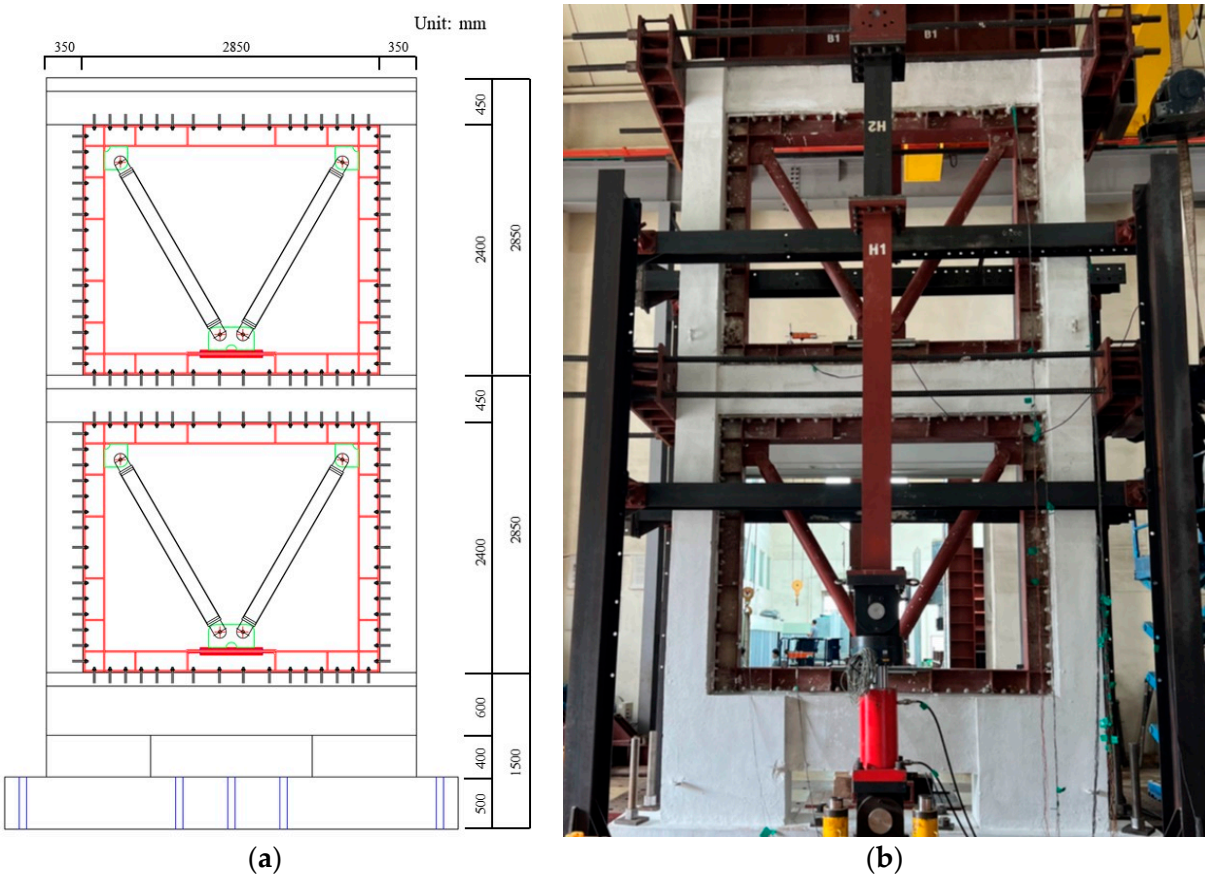

Figure 16. Detailed configuration of the specimens strengthened using the LLFD-V typed seismic control system (PD-LLFD-V): (**a**) specimen details; (**b**) photography.

Table 10. Summary of the specimen details.

Specimens	Test Methods	Strengthening Types	Earthquake Levels (cm/s^2)
PD-RC	Pseudo-dynamic	Non	200
PD-LLFD-V	Pseudo-dynamic	LLFD-V typed seismic control system	200/300/400/500
Notation	PD	RC LLFD-V	PD: Pseudo-dynamic test RC: R/C Frame without strengthening LLFD-V: R/C Frame strengthened using the LLFD V-typed seismic control system

4.5. Experiment Results and Analysis

The crack and failure results for the two specimens (the non-reinforced pseudo-dynamic specimen (PD-RC) and the pseudo-dynamic specimen retrofitted with the LLFD V-bracing system (PD-LLFD-V)) were determined. The seismic retrofitting effect of the PD-LLFD-V compared to the PD-RC was verified by analyzing the load–displacement curves (restoring force), time history curves for displacement, and maximum seismic responses.

4.5.1. Crack and Failure Geometry

(1) PD-RC

Figure 17 shows the crack and failure situations of PD-RC after the input ground motion of 200 cm/s^2. According to the figure, initial bending cracks occurred at the bottom of the columns in approximately 2.08 s (displacement: 6.4 mm) for PD-RC. At 2.4 s (displacement: 16.9 mm), the bending cracks propagated, and shear cracks occurred at the top and bottom of the columns. After 3.45 s (displacement: 66.5 mm), the widths of the

shear cracks at the bottom of the columns increased. The maximum displacement occurred at 5.35 s (displacement: 67.3 mm), and severe peeling of the concrete began, along with a serious increase in the widths of the shear cracks. Finally, shear failure occurred at the bottom of the frame on the first floor, resulting in the final collapse.

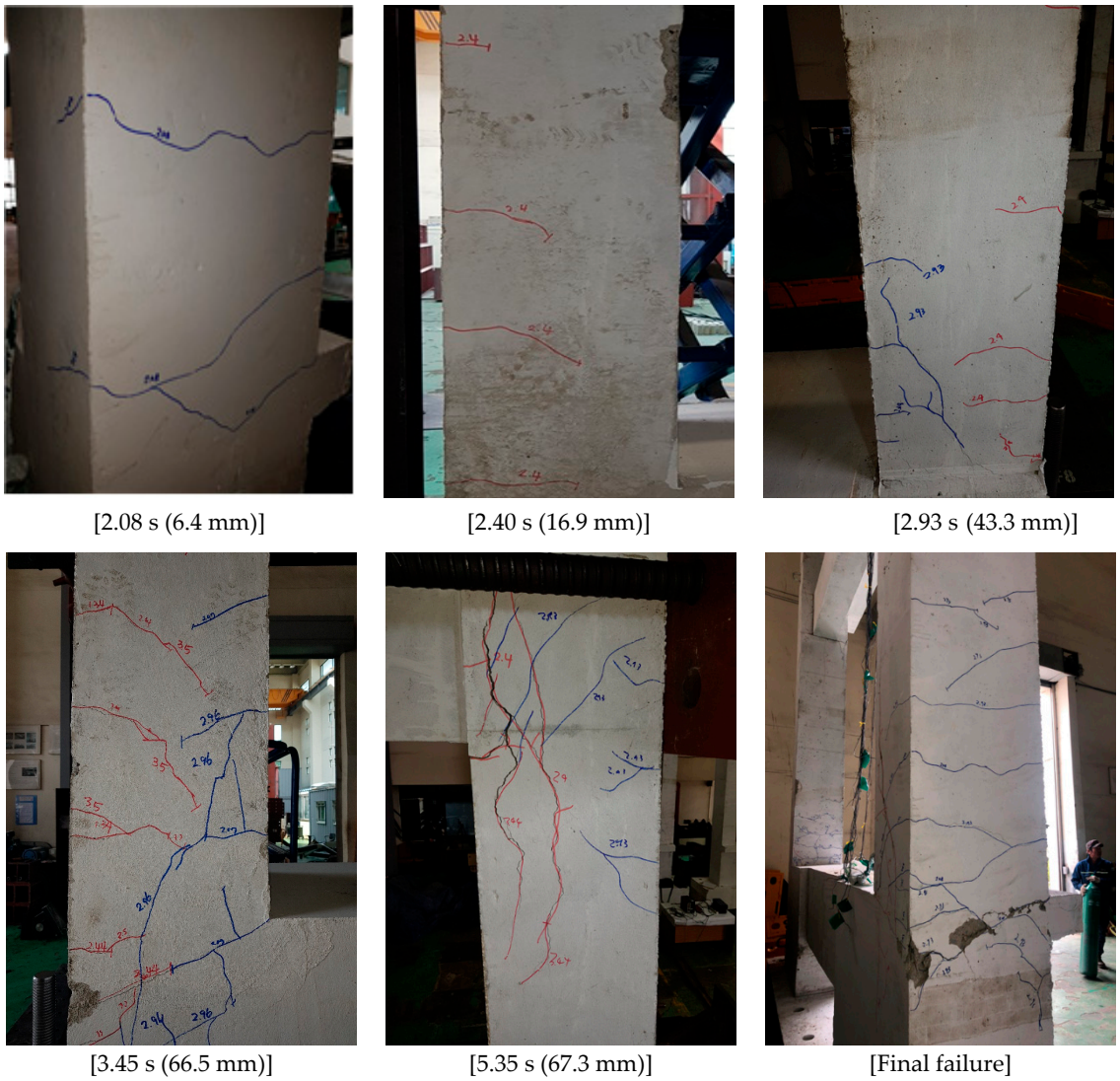

Figure 17. Cracks and final failures of non-strengthened frame specimen (PD-FR) (200 cm/s^2).

These results are consistent with the results of a previous study [47] that found that significant seismic damage could occur to school buildings with non-seismic details in the event of an earthquake of 200 cm/s^2. These significant results highlight the need for seismic retrofitting of R/C school buildings constructed in the 1980s with non-seismic details.

(2) PD-LLFD-V

Figures 18–21 show the crack and final test situations of PD-LLFD-V after input ground motions of 200–500 cm/s^2. For the PD-LLFD-V specimen, fine initial bending cracks occurred at the bottom of the columns at approximately 2.28 s (displacement: 2.8 mm) under the input ground motion of 200 cm/s^2, as shown in Figure 18. After 3.07 s (displacement: 5.4 mm), the number of bending cracks increased, and fine cracks were observed. At 3.57 s (displacement: 9.6 mm), when the maximum response was observed, fine bending cracks also occurred. Consequently, the specimen retrofitted with the LLFD V-bracing system showed fine bending cracks under an earthquake of 200 cm/s^2, which caused the shear failure of the non-reinforced specimen, thereby confirming the retrofitting effect.

[2.28 s (2.8 mm)] [3.07 s (5.4 mm)] [3.57 s (9.6 mm)] [6.25 s (7.0 mm)]

Figure 18. Cracks of LLFD-strengthened frame specimen (200 cm/s^2).

[2.29 s (8.4 mm)] [3.55 s (9.6 mm)] [3.59 s (15.7 mm)] [6.25 s (15.1 mm)]

Figure 19. Cracks of LLFD-strengthened frame specimen (300 cm/s^2).

[2.6 s (19.7 mm)] [3.23 s (21.6 mm)] [3.61 s (27.1 mm)] [6.28 s (24.5 mm)]

Figure 20. Cracks of LLFD-strengthened frame specimen (400 cm/s^2).

[2.66 s (29.9 mm)] [3.26 s (31.3 mm)] [3.62 s (36.3 mm)] [Final failure]

Figure 21. Cracks and final scene of LLFD-strengthened frame specimen (500 cm/s^2).

As seen in Figure 19, with an input ground motion of 300 cm/s^2, the number of bending cracks after 2.29 s (displacement: 8.4 mm) was greater than that with 200 cm/s^2. After 3.59 s (displacement: 15.7 mm), when the maximum response was observed, bending cracks occurred on a small scale. Therefore, the failure mode was finally determined by bending cracks. The non-reinforced specimen shown in Figure 17 exhibited a typical shear failure frame. For the PD-LLFD-V specimens, however, the failure mode changed from shear failure to bending failure.

As seen in Figure 20, with an input ground motion of 400 cm/s^2, a greater number of bending cracks were observed after 3.23 s (displacement: 21.6 mm) compared to those with 300 cm/s^2. Shear cracks also occurred at the same time, but they were insignificant. The width and number of bending cracks increased even after 3.61 s (displacement: 27.1 mm) when the maximum response occurred, but the shear cracks were insignificant. Therefore, the final failure mode was determined by bending cracks. As seen in Figure 21, with an input ground motion of 500 cm/s^2, a greater number of bending and shear cracks were observed after 2.66 s (displacement: 29.9 mm) compared to those with 400 cm/s^2. After 3.62 s (displacement: 36.3 mm), bending and shear cracks significantly propagated. Finally, the failure mode was determined by bending and shear cracks.

4.5.2. Maximum Seismic Response Load and Displacement

Table 11 compares the experiment results for the maximum response loads and displacements of the PD-RC specimen under the input ground motion of 200 cm/s^2 and the PD-LLFD-V specimen under 200–500 cm/s^2 with the failure modes and seismic damage scales. According to the pseudo-dynamic test results for the PD-RC specimen, a maximum seismic response value of 251.4 kN (displacement: 67.3 mm) was observed under the input ground motion of 200 cm/s^2, and the target frame showed shear failure at approximately 5.35 s when the maximum seismic response occurred. The seismic damage scale was determined to be the collapse level according to JBDPA [48] and Maeda et al. [49].

Meanwhile, the PD-LLFD-V specimen exhibited a maximum seismic response shear force of 439.7 kN (displacement: 9.6 mm) under 200 cm/s^2. Consequently, the specimen retrofitted with the LLFD V-bracing system showed minor seismic damage. Under 300 cm/s^2, which caused a maximum seismic response of 610.9 kN (displacement: 15.7 mm), a low degree of damage occurred, according to JBDPA [48] and Maeda et al. [49]. Compared to the non-reinforced frame that showed the shear failure mode, the failure mode was changed from shear failure to bending failure, confirming that the developed LLFD vibration control system has an excellent seismic energy dissipation capacity. In the cases of 400 and 500 cm/s^2, which assumed a large earthquake, maximum seismic response shear forces of 756.6 kN (maximum displacement: 27.1 mm) and 883.6 kN (maximum displacement: 36.3 mm) were observed. The degree of seismic damage was judged to be

at the medium level, with the validity of the seismic retrofitting effect verified for large earthquakes at the 2400-year return period level.

Table 11. Maximum response load–displacement and extent of earthquake-induced damage.

Specimen	Earthquake Wave	Input Ground Acceleration [cm/s^2]	Maximum Load V_u [kN]	Maximum Displacement δ_u [mm]	Degree of Damage * (Failure Mode)
PD-RC	Hachinohe (EW)	200	251.4	67.3	Collapse (shear failure)
PD-LLFD-V	Hachinohe (EW)	200	439.7	9.6	Light (flexural crack)
		300	610.9	15.7	Small (flexural crack)
		400	756.6	27.1	Medium (flexural shear failure)
		500	883.6	36.3	Medium (flexural shear failure)

* Degree of earthquake-induced damage was evaluated based on JBDPA [48] and Maeda et al. [49].

4.5.3. Analysis of the Load–Displacement and Displacement–Time History Results

Figure 22 shows the load–displacement curve of the non-reinforced specimen for 200 cm/s^2 and the load–displacement curve of the reinforced specimen (PD-LLFD-V) for 200–500 cm/s^2. Figure 23 compares the seismic response displacement–time history curves of the non-reinforced (200 cm/s^2) and reinforced specimens (200–500 cm/s^2). Table 12 compares the seismic response strength ratios and displacement ratios, which are important factors for seismic performance assessment, from the experiment results for the reference (200 cm/s^2) and reinforced specimens (200–500 cm/s^2).

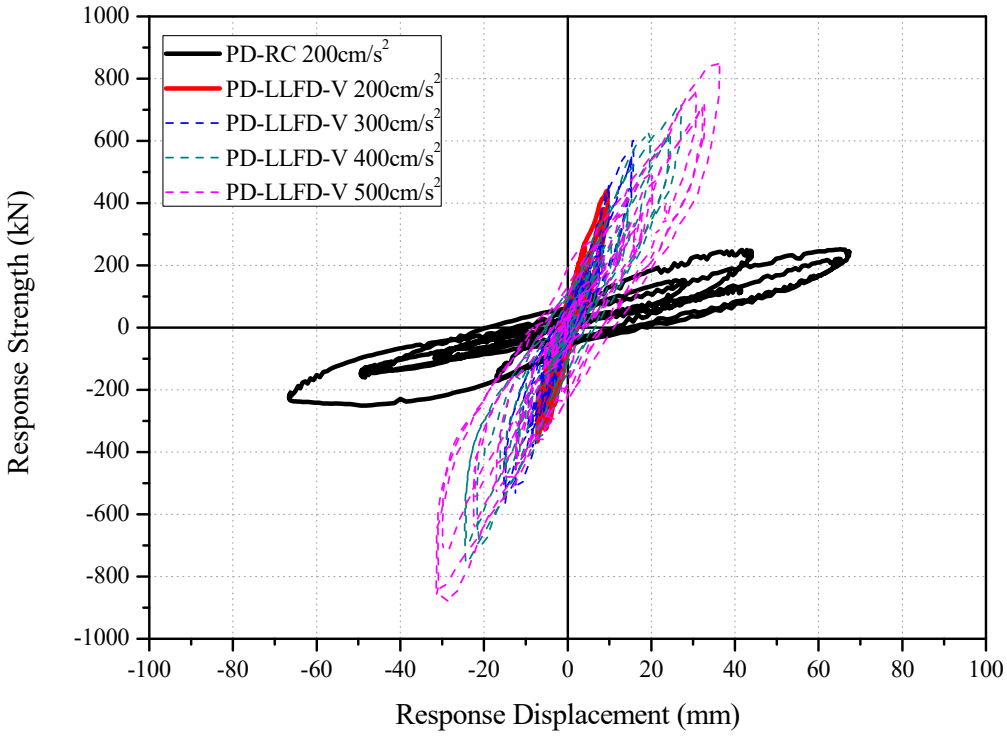

Figure 22. Comparison of shear strength and displacement of seismic response.

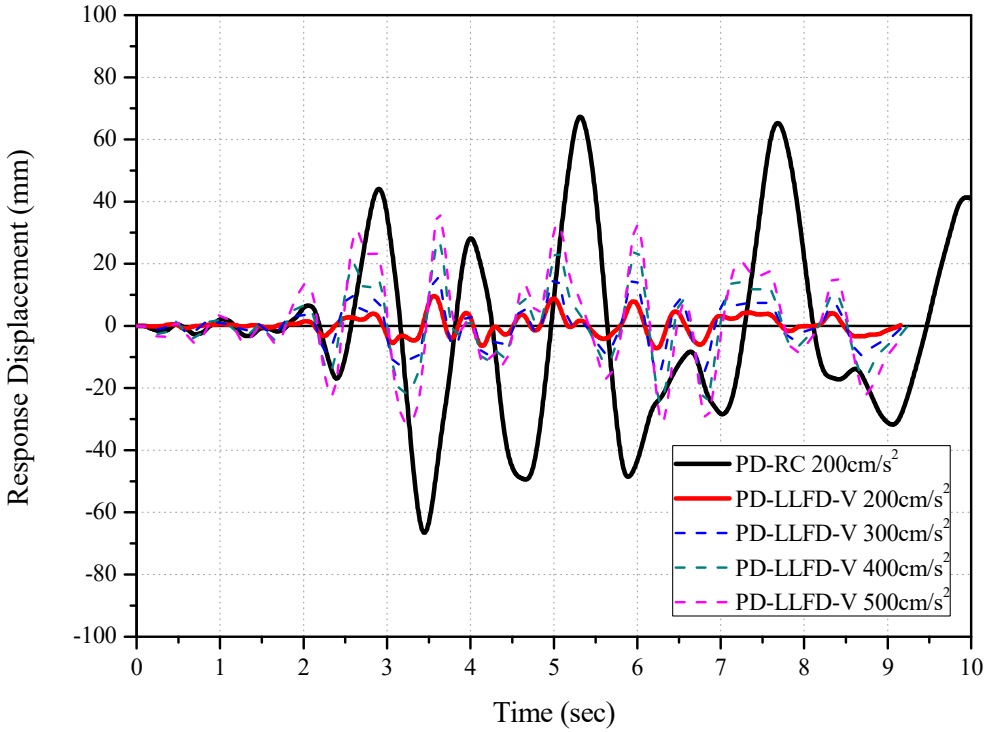

Figure 23. Comparison of time and displacement of seismic response.

Table 12. Comparison of strength ratio and displacement ratio of seismic response.

Specimen	Earthquake Wave	Input Ground Acceleration [cm/s^2]	Seismic Response Load		Seismic Response Displacement	
			Maximum Load V_u [kN]	Maximum Strength Ratio R_s *1	Maximum Displacement δ_u [mm]	Displacement Ratio R_d *2
PD-RC	Hachinohe (EW)	200	251.4	1.00 (251.4/251.4)	67.3	1.00 (67.3/67.3)
PD-LLFD-V	Hachinohe (EW)	200	439.7	1.74 (439.7/251.4)	9.6	0.14 (9.6/67.3)
		300	610.9	2.42 (610.9/251.4)	15.7	0.23 (15.7/67.3)
		400	756.6	3.00 (756.6/251.4)	27.1	0.40 (27.1/67.3)
		500	883.6	3.51 (883.6/251.4)	36.3	0.54 (36.3/67.3)

*1 R_s: Maximum strength ratio of the NBSD-strengthened specimen relative to the non-strengthened specimen. *2 R_d: Maximum displacement ratio of the NBSD-strengthened specimen relative to the non-strengthened specimen.

According to the above-mentioned figures and table, the LLFD method increased the seismic response strength by approximately 1.74 times under the input ground motion of 200 cm/s^2, 2.42 times under 300 cm/s^2, 3.00 times under 400 cm/s^2, and 3.51 times under 500 cm/s^2 compared to the reference specimen (PD-RC). These results are also well reflected in Figures 16–20, which compare the final failure situations. Compared to the reference specimen, the LLFD method increased the displacement response ratio by approximately 0.14 times for 200 cm/s^2, 0.23 times for 300 cm/s^2, 0.40 times for 400 cm/s^2, and 0.54 times for 500 cm/s^2. The seismic response displacement for the same seismic load (200 cm/s^2) was suppressed by approximately 86%, confirming the excellent seismic energy absorption capacity and validity of the proposed LLFD method.

5. Comparison of the Pseudo-Dynamic Test and Non-Linear Dynamic Analysis Results

Based on the results of the LLFD member test and pseudo-dynamic test discussed in Sections 3 and 4, restoring force characteristics were proposed for the beams, columns, and reinforcement (LLFD) for a non-linear dynamic analysis of the two-story frame retrofitted with the LLFD V-bracing system. A non-linear dynamic analysis was conducted on the two-story pseudo-dynamic test specimen based on the proposed restoring force characteristics, with the results obtained compared with the pseudo-dynamic test results.

5.1. Non-Linear Dynamic Analysis Overview

The target specimens used in the non-linear dynamic analysis were the non-reinforced two-story R/C frame, with the frame retrofitted with the LLFD V-bracing system shown in Figures 15 and 16 in Section 4.4. While the actual structures vibrate in three dimensions, in this study, they were modeled as plane frames that considered only horizontal seismic forces by replacing columns, beams, and walls with linear elements. The floor characteristics of the structure were evaluated based on the member level, with the following assumptions made for the analysis: (1) The location of the yield hinge of each member was determined by referring to the literature [50,51], with the section from the center of each member to its end where the yield hinge occurred assumed to be rigid; and (2) The strength of the beams also considered the influence of slab reinforcing bars within the effective width of the slab, which was the scope of the cooperation with the beams. In addition, each member was modeled as serially connected flexural, shear, and axial springs, as shown in Figure 24.

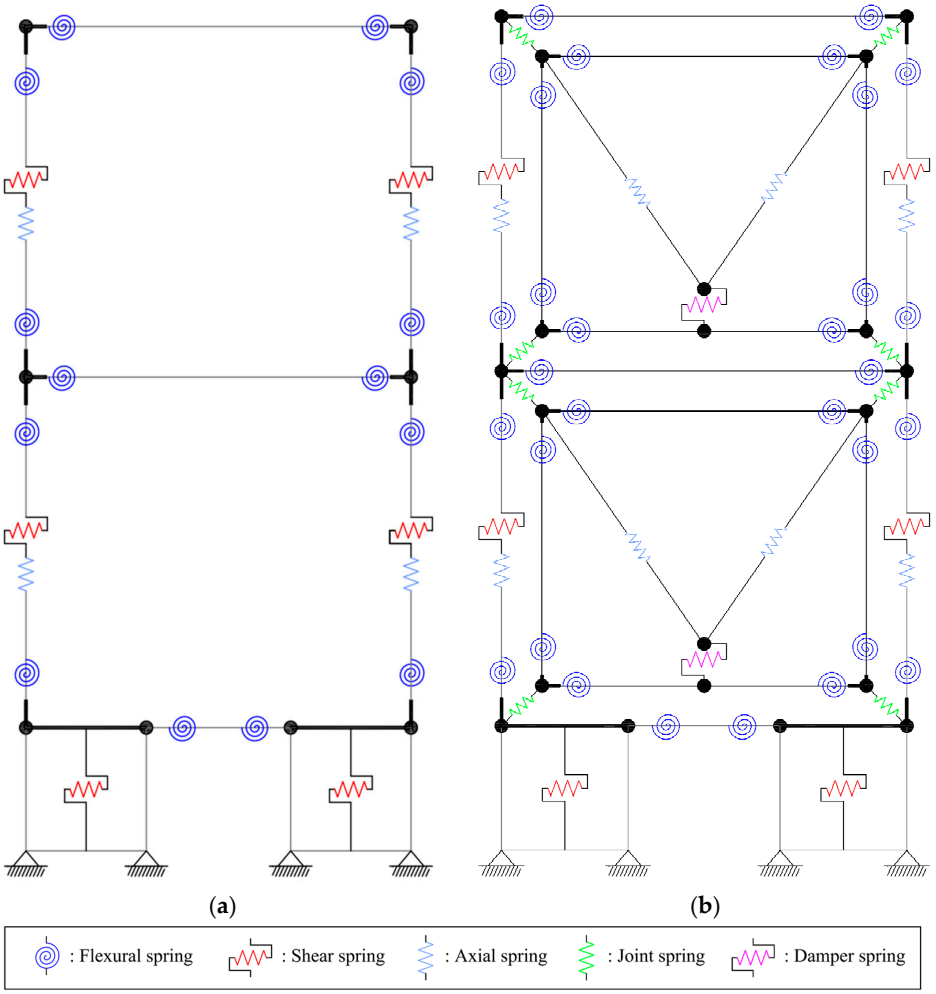

Figure 24. Nonlinear dynamic analysis model: (**a**) Non-strengthened frame (PD-RC); (**b**) LLFD V-typed strengthening frame (PD-LLFD-V).

As for the restoring force model of the LLFD vibration control system, the perfect plastic (PP) model was applied based on the LLFD member test results shown in Section 3. In the case of the hysteretic characteristics of the PP model, the characteristics of the unloading and reloading hysteresis curves were determined by the initial stiffness (K_0) and yield strength of the LLFD ($V_{d,y}$). Table 13 lists the parameters of the PP model used for the LLFD, while Figure 25 shows the LLFD restoring force characteristics for the non-linear dynamic analysis based on Table 13. The LLFD was the GS-LLFD used in the pseudo-dynamic test. The torque pressure was T_0 = 200kN·m and the yield strength ($V_{d,y}$) was 125 kN, obtained using regression Equation (4) for the member test. The yield displacement ($\delta_{d,y}$) was 0.08 mm, as measured in the member test (see Table 4).

Table 13. Parameters of perfect plastic model used in LLFD.

Member	T_0 (kN·m)	$\delta_{d,y}$ [mm]	$V_{d,y}$ [kN]	K_0 [kN/mm]
LLFD	200	0.08	125	15,625

T_0: Torque, $\delta_{d,y}$: Yield displacement, $V_{d,y}$: Yield strength, K_0: Initial stiffness.

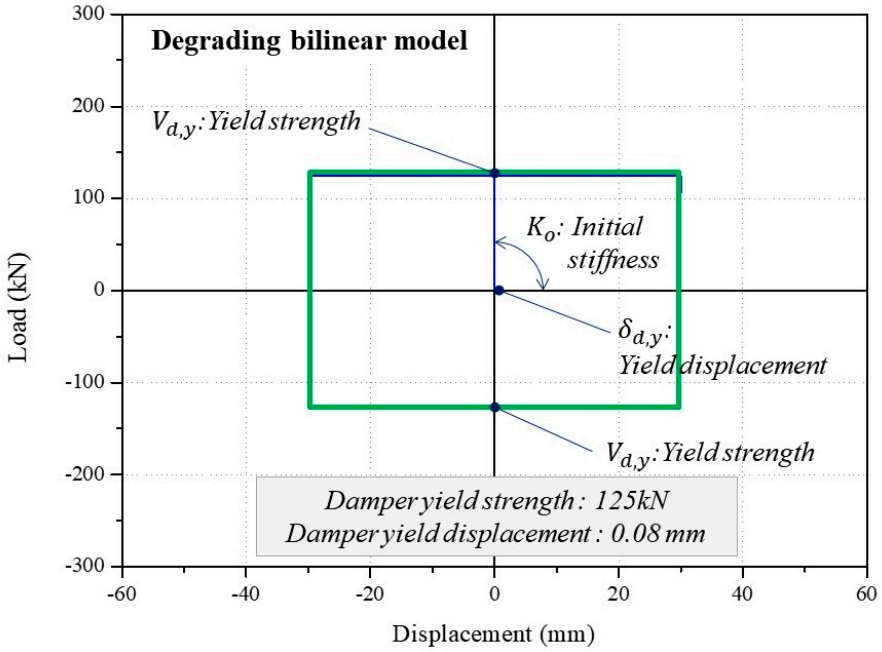

Figure 25. Hysteresis model of LLFD for nonlinear dynamic analysis.

The non-reinforced frame specimen, with ground beams and walls at the foundation (Figure 24a), comprised 12 nodes, including two bottom plates and ground points. Meanwhile, the frame specimen retrofitted with the LLFD V-bracing system (PD-LLFD-V) consisted of nodes that connected the additional steel frame to the existing R/C frame, LLFD, and V-shaped steel member for the LLFD installation, as shown in Figure 24b. The PD-LLFD-V frame had 24 nodes, including ground points. The joint between the existing R/C member and steel frame was modeled with a link joint element.

For the axial force in the non-linear dynamic analysis, the axial load applied to the actual existing frame (two columns) used in the pseudo-dynamic test shown in Figures 14 and 15 (i.e., 1000 kN) was distributed to the upper beam–column joint nodes, and a constant axial force of 500 kN was applied. The additional weight of the R/C frame and LLFD reinforcement was also applied to the corresponding nodes.

The non-linear dynamic analysis was conducted using CANNY (Version C11), a general-purpose software program for three-dimensional non-linear dynamic analysis developed by Li [52]. Table 14 provides an overview of the restoring force characteristics

of each member used in the non-linear dynamic analysis. The variables that determined the restoring force characteristics of each column and beam shown in Table 14 (i.e., the initial flexural stiffness (k_B), initial shear stiffness (k_s), flexural crack moment (M_c), shear crack strength (V_c), flexural ultimate strength (M_u), and shear ultimate strength (V_u)) were determined using Equations (9)–(17) based on the research results of JBDPA [50] and AIJ [51].

Table 14. Restoring force characteristics of each member used in non-linear dynamic analysis.

Member	Restoring Force Model		Model Name
Beam	Flexural spring	CP3	Cross-peak trilinear model
	Shear spring	OO3	Trilinear origin-oriented
Column	Flexural spring	CA7	CANNY sophisticated trilinear hysteresis model
	Shear spring	OO3	Trilinear origin-oriented
	Axial spring	AS1	Axial stiffness model
Wall	Shear spring	OO3	Trilinear origin-oriented
Anchor bolt	Shear spring	EL2	Bilinear elastic model
LLFD	Damper spring	PP	Perfect Plastic model
Steel frame	Flexural spring	BL2	Degrading bilinear model
	Shear spring	EL2	Bilinear elastic model

$$M_c = 0.63\sqrt{F_c}Z\phi \text{ (Beam)} \tag{9}$$

$$M_c = 0.63\sqrt{F_c}Z + ND/6 \text{ (Column)} \tag{10}$$

$$M_u = 0.9a_t\sigma_y d \text{ (Beam)} \tag{11}$$

$$M_u = 0.8a_t\sigma_y D + 0.5ND(1 - \frac{N}{bDF_c}) \text{ (Column)} \tag{12}$$

$$k_B = 6EI/l \text{ (Both beam and column)} \tag{13}$$

Here, M_c is the flexural crack moment (N·mm), M_u is the ultimate flexural moment (N·mm), k_B is the initial flexural stiffness (N/mm), F_c is the compressive strength of the concrete (N/mm^2), Z is the section modulus (mm^3), ϕ is the shape factor of the beam, N is the axial force (N), D is the column depth (mm), a_t is the total cross-sectional area of the tensile reinforcing bars (mm^2), σ_y is the yield strength of the reinforcing bars (N/mm^2), and d is the effective depth (mm).

$$V_c = \{\frac{(1 + \frac{\sigma_0}{15})0.065k_c(50 + F_c)}{\frac{M}{Vd} + 1.7}\}bj \text{ (Both beam and column, if beam, } \sigma_0 = 0) \tag{14}$$

$$V_u = \left\{\frac{0.053p_t^{0.023}(18 + F_c)}{\frac{M}{Vd} + 0.12} + 0.85\sqrt{p_{ws} \cdot \sigma_{wy}} + 0.1\sigma_0\right\}bj \text{ (Both beam and column, if beam, } \sigma_0 = 0) \tag{15}$$

$$k_s = GA/\kappa \text{ (Both beam and column)} \tag{16}$$

Here, V_c is the shear crack strength (N·mm); V_u is the ultimate shear strength (N); k_B is the initial shear stiffness (N/mm); σ_0 is the axial stress in the column (N/mm^2); k_c is the modification coefficient, which depends on the cross-section; b is the width (mm); j is the distance between the centroids of the tensile and compressive forces (mm); p_t is the tensile reinforcement ratio (percent); p_{ws} is the shear reinforcement ratio (p_{ws} = 0.012

for $p_{ws} \geq 0.012$); σ_{wy} is the yield strength of the shear reinforcing bars (N/mm^2); M/V is the shear span length, which had a default value of $h_o/2$; h_o is the clear height of the column (mm).

Meanwhile, the restoring force characteristics of the shear-failure-type column with non-seismic details (shear spring, OO3 in Table 14) were determined using Equation (17), proposed based on the structural testing of columns with non-seismic details in Korea [53].

$$V_u = 2.5V_c : \delta_u = 5\delta_c \quad (17)$$

Here, V_u is the ultimate strength at the time of shear failure, V_c is the strength at the time of shear cracking, δ_u is the displacement at the time of shear failure, and δ_c is the displacement at the time of shear cracking.

5.2. Comparison of the Non-Linear Dynamic Analysis and Pseudo-Dynamic Test Results

The non-linear dynamic analysis was conducted using CANNY based on the model described in Section 5.1 with Hachinohe (EW) seismic waves of 200, 300, and 400 cm/s^2, which were used in the pseudo-dynamic test. As mentioned above, the Hachinohe (EW) seismic wave of 200 cm/s^2 was applied to the non-reinforced specimen in the pseudo-dynamic test, while 200, 300, and 400 cm/s^2 were applied to the LLFD-reinforced specimen.

Figure 26 shows the seismic response load–displacement and time–displacement hysteresis curves for the first floor based on the non-linear dynamic analysis and pseudo-dynamic test of the non-reinforced specimen subjected to 200 cm/s^2.

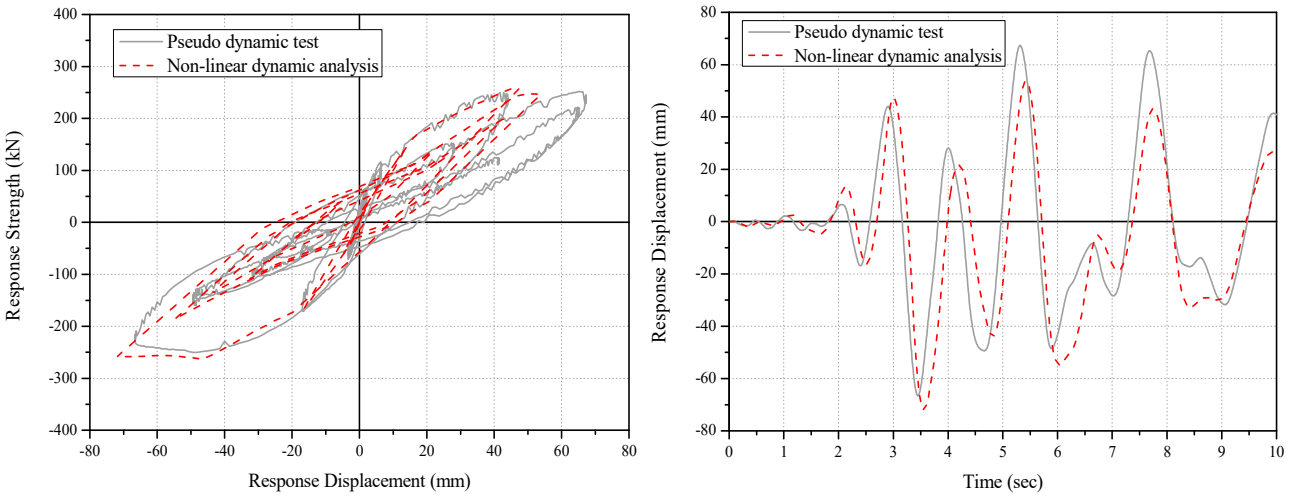

Figure 26. Comparison of seismic response load–displacement and displacement hysteresis based on pseudo-dynamic test and nonlinear dynamic analysis of non-strengthened specimen (1F, 200 cm/s^2).

Figures 27–29 show the seismic response load–displacement and time–displacement hysteresis curves for the first floor based on the non-linear dynamic analysis and pseudo-dynamic test of the specimen retrofitted with the LLFD V-bracing system and subjected to 200–400 cm/s^2. In addition, Figures 30–32 show the seismic response load–displacement and time–displacement hysteresis curves for the LLFD subjected to 200–400 cm/s^2. In the load–displacement curves shown in Figures 30–32, a yield strength ($V_{d,y}$) of 125 kN was used, the same as in the non-linear dynamic analysis, because no load on the LLFD was measured in the pseudo-dynamic test. Table 15 compares the maximum response load–maximum response displacement relationships based on the non-linear dynamic analysis and pseudo-dynamic test.

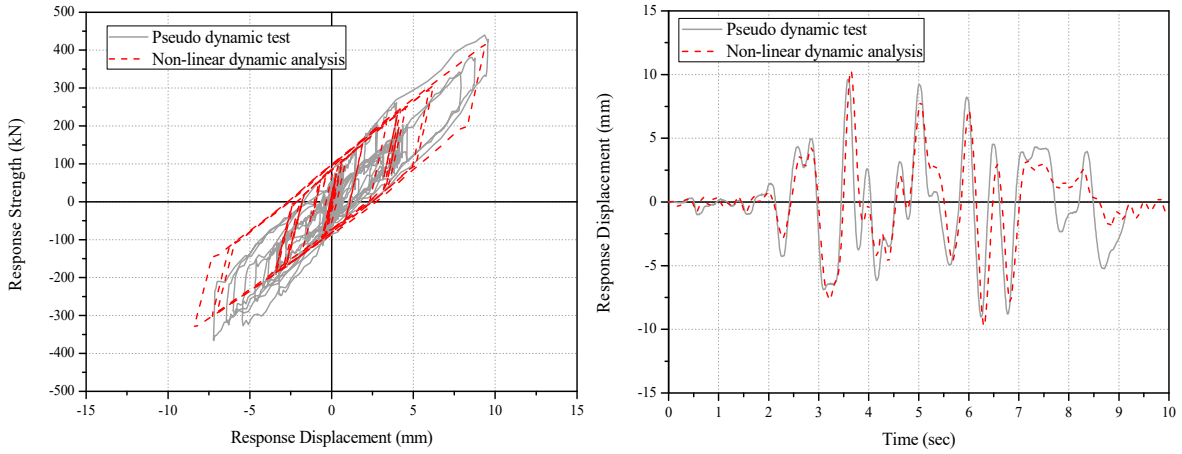

Figure 27. Comparison of seismic response load–displacement and displacement hysteresis based on pseudo-dynamic test and nonlinear dynamic analysis of LLFD-strengthened specimen (1F, 200 cm/s^2).

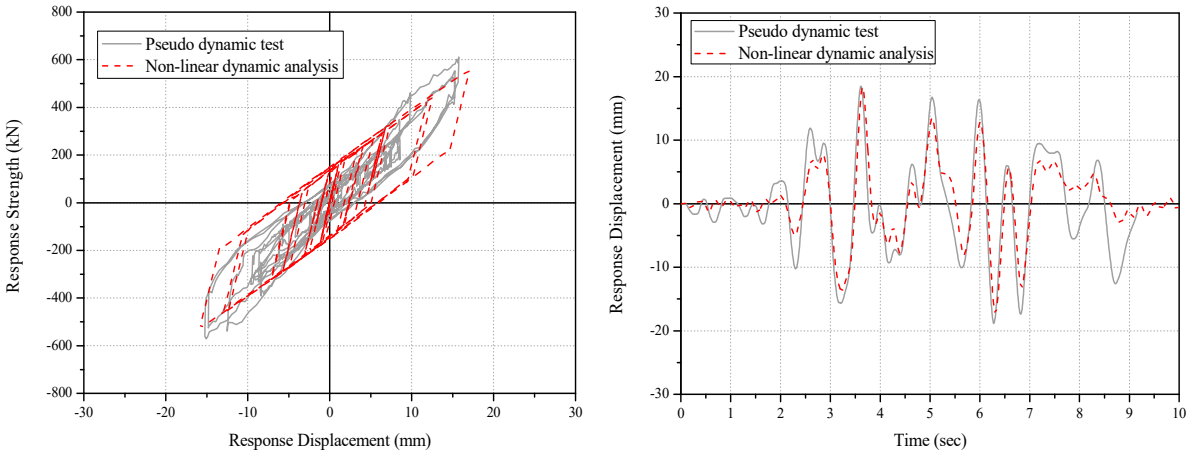

Figure 28. Comparison of seismic response load–displacement and displacement hysteresis based on pseudo-dynamic test and nonlinear dynamic analysis of LLFD-strengthened specimen (1F, 300 cm/s^2).

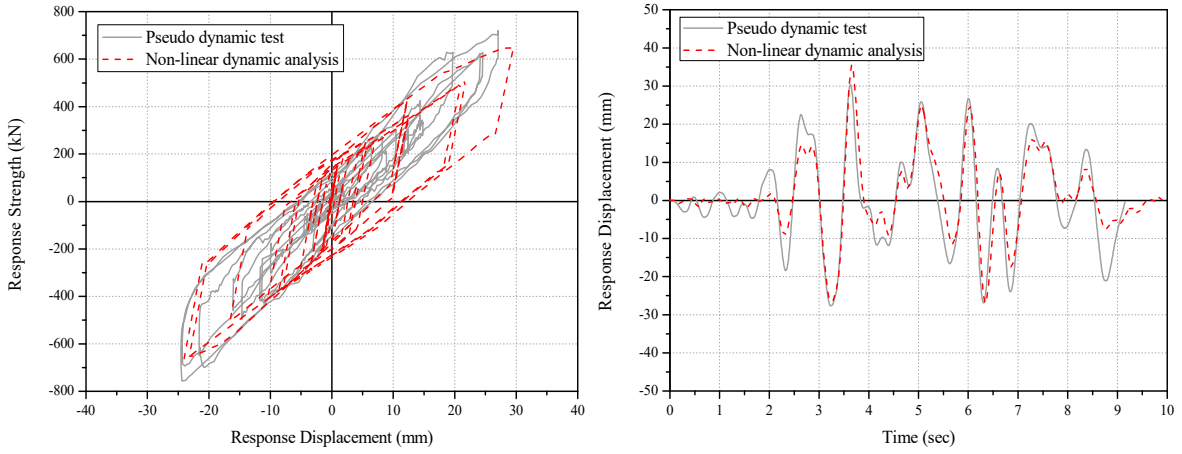

Figure 29. Comparison of seismic response load–displacement and displacement hysteresis based on pseudo-dynamic test and nonlinear dynamic analysis of LLFD-strengthened specimen (1F, 400 cm/s^2).

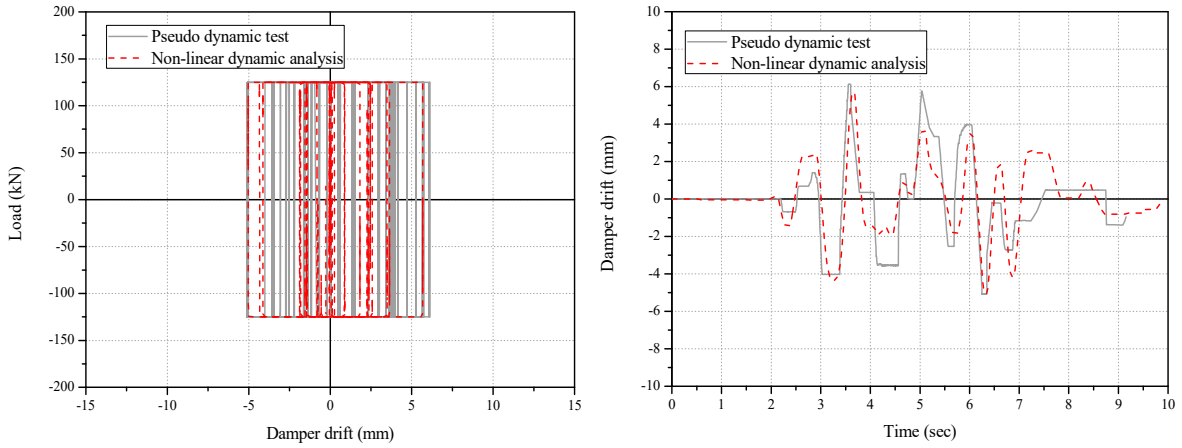

Figure 30. Comparison of seismic response load–displacement and displacement hysteresis based on pseudo-dynamic test and nonlinear dynamic analysis of LLFD (1F, 200 cm/s^2).

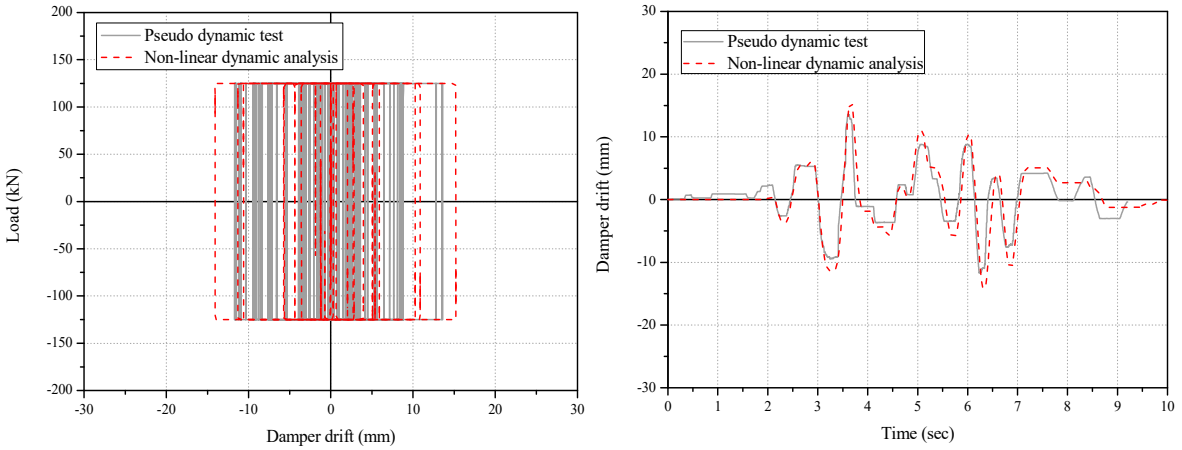

Figure 31. Comparison of seismic response load–displacement and displacement hysteresis based on pseudo-dynamic test and nonlinear dynamic analysis of LLFD (1F, 300 cm/s^2).

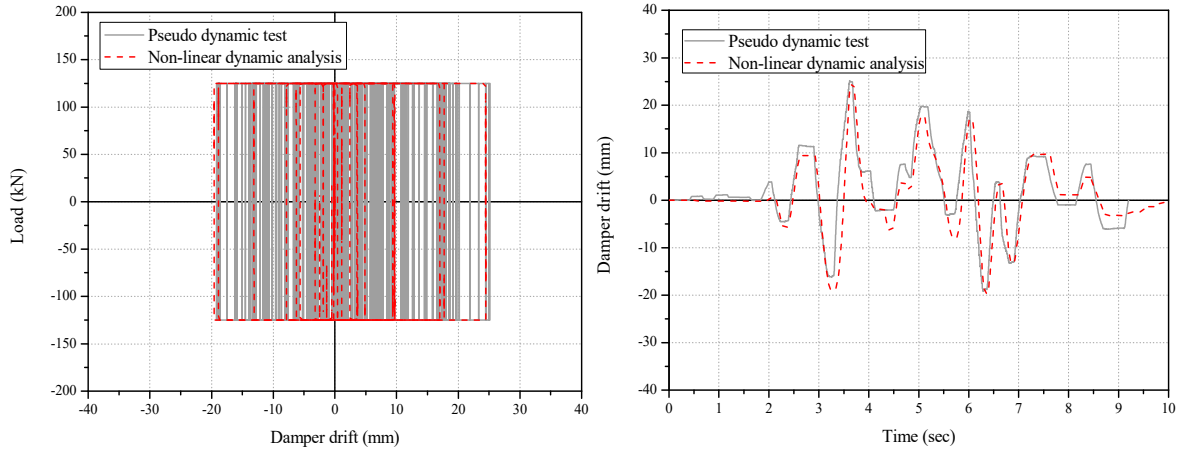

Figure 32. Comparison of seismic response load–displacement and displacement hysteresis based on pseudo-dynamic test and nonlinear dynamic analysis of LLFD (1F, 400 cm/s^2).

Table 15. Correlation of maximum response load and maximum response displacement based on nonlinear dynamic analysis and pseudo-dynamic test.

Specimen	Input Ground Acceleration [cm/s^2]	Method	Maximum Displacement [mm]	Maximum Displacement Deviation Ratio [Analysis/Test]	Maximum Load [kN]	Maximum Load Deviation Ratio [Analysis/Test]
PD-RC	200	PDT	67.3	1.07	251.4	1.05
		NDA	71.9		263.1	
PD-LLFD-V	200	PDT	9.5	0.99	439.6	0.95
		NDA	9.4		416.5	
	300	PDT	15.7	1.08	610.9	0.91
		NDA	17.0		553.0	
	400	PDT	27.1	1.09	756.6	0.88
		NDA	29.5		662.6	

Note: PDT: Pseudo-dynamic test, NDA: Nonlinear dynamic analysis.

Under an input seismic acceleration of 200 cm/s^2, the maximum seismic response load and displacement values for PD-RC were 263.1 kN and 71.9 mm in the non-linear dynamic analysis and 251.4 kN and 67.3 mm in the pseudo-dynamic test, respectively (Figure 26 and Table 15). Under 200 cm/s^2, the maximum seismic response load and displacement values for PD-LLFD-V were 416.5 kN and 9.4 mm in the non-linear dynamic analysis and 439.6 kN and 6.5 mm in the pseudo-dynamic test, respectively (Figure 27 and Table 15).

Under 300 cm/s^2, the maximum seismic response load and displacement values were 553.0 kN and 17.0 mm in the non-linear dynamic analysis and 610.9 kN and 15.7 mm in the pseudo-dynamic test, respectively (Figure 28 and Table 15). Under 400 cm/s^2, which assumed a large earthquake, the maximum seismic response load and displacement values were 662.6 kN and 29.5 mm in the non-linear dynamic analysis and 756.6 kN and 27.1 mm in the pseudo-dynamic test, respectively (Figure 29 and Table 15). Overall, for the ground motion with 200–400 cm/s^2, the non-linear dynamic analysis and pseudo-dynamic test results were similar, with an average difference of less than 10%. The above accuracy for the seismic response load and displacement could also be observed in the seismic response load–displacement relationship of the LLFD, as shown in Figures 30–32.

These non-linear dynamic analysis results showed that the non-linear analysis model and method developed in this study could effectively simulate the LLFD method and seismic behavior of an R/C frame retrofitted with this method, thus confirming that the seismic retrofitting effect of the developed LLFD method could be effectively evaluated based on the analysis model and method discussed in Section 5.1.

6. Evaluation of Seismic Retrofitting and Seismic Performance of R/C Building Retrofitted with LLFD V-Bracing System

6.1. Non-Linear Dynamic Analysis Overview

The non-linear analysis model and method discussed in Section 5 could effectively simulate the seismic behavior of an R/C frame retrofitted with the LLFD V-bracing system. For evaluating the commercialization potential of the LLFD V-bracing system, based on the analysis model and method discussed in Section 5.1, a non-linear dynamic analysis was conducted on an R/C school building with non-seismic details (see Figure 14) retrofitted with the LLFD V-bracing system. The seismic response load and displacement characteristics of the building before and after seismic retrofitting were evaluated, with the seismic retrofitting effect verified by examining the energy dissipation capacity, seismic response load, and response displacement characteristics of the damper.

As discussed in Section 5, a non-linear dynamic analysis was conducted using CANNY [52]. This analysis was conducted using the Hachinohe (EW) 200 cm/s^2 setting

as the input ground motion, which was the level used for the seismic design of the target building and caused the collapse of a non-reinforced frame. Figure 33 shows the modeling of the target R/C school building before and after retrofitting. The seismic reinforcement volume required for the LLFD V-bracing system was calculated using Equations (18)–(20), which could be used to determine the seismic energy absorption effect of the vibration control system based on the method proposed by the Japan seismic diagnosis standards [50], i.e., Newmark's equal energy criterion [54,55].

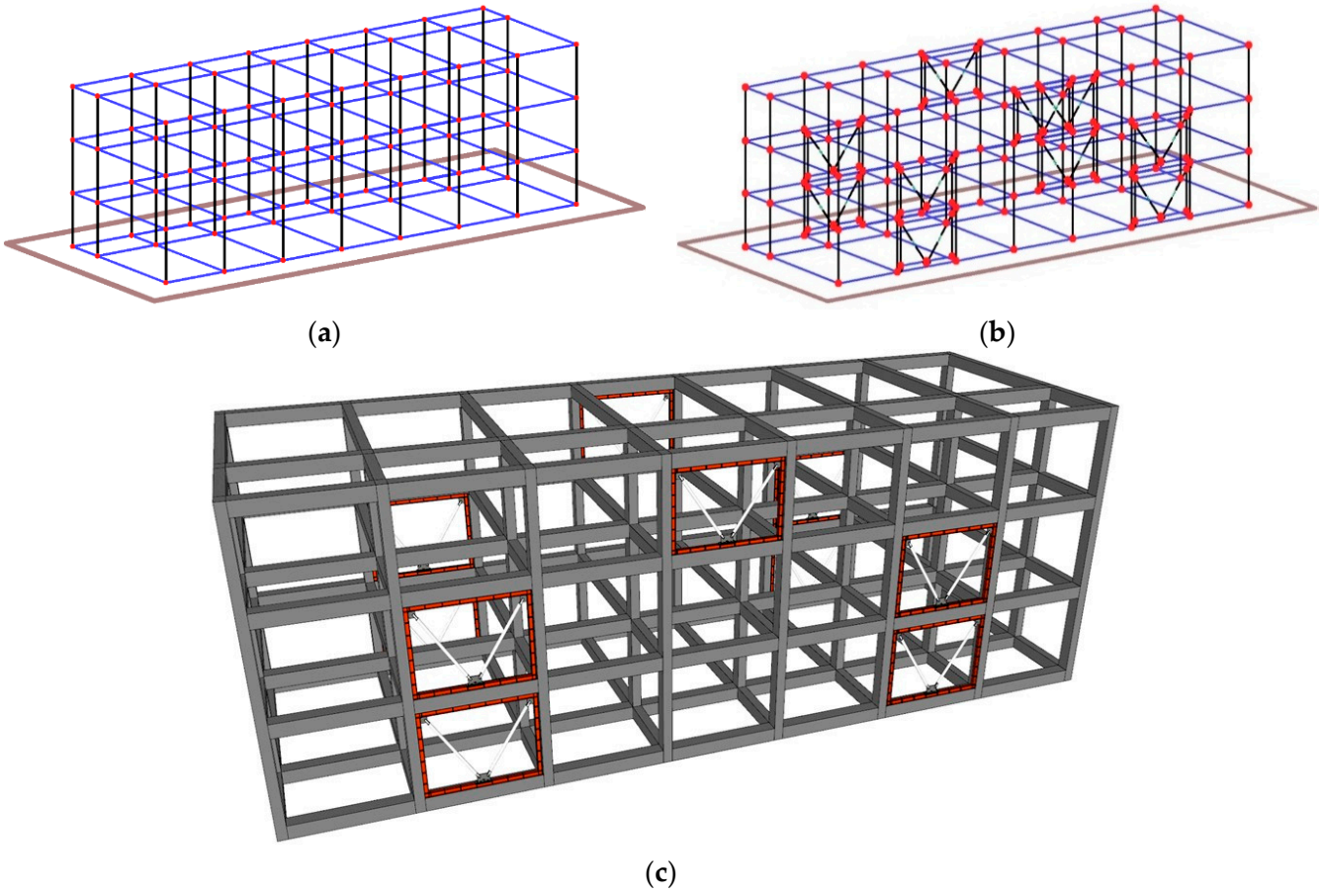

Figure 33. Modeling of the R/C school building before and after seismic strengthening: (**a**) Frame without strengthening; (**b**) Frame with LLFD V-typed strengthening; (**c**) Frame with LLFD V-typed strengthening (Isometric view).

$$Q_{ydp} = \frac{\left[\left(\frac{E_{Ro}}{E_o}\right)^2 - 1\right] \cdot \phi^2 \cdot (2\mu - 1) \cdot \mu_{dp}}{2\beta \cdot \left(\mu \cdot \mu_{dp} - 1\right)} \cdot Q_{yst} \tag{18}$$

$$E_{Ro} = C_{yst} \cdot \sqrt{\phi^2(2\mu - 1) + 2\beta \cdot \alpha_c \left(\mu - \frac{\alpha_c}{\alpha_k}\right)} \tag{19}$$

$$E_o = C_{yst} \cdot \sqrt{\phi^2(2\mu - 1)} \tag{20}$$

Here, Q_{ydp} is the seismic reinforcement volume required for the damper (required strength), Q_{yst} is the yield strength of the existing structural member, E_{Ro} is the target basic performance index after seismic retrofitting, E_o is the basic performance index of the existing structural member, ϕ is the coefficient for calculating the ductility index of the existing R/C structure ($= 1/0.75(1 + 0.05\mu)$), μ is the ductility ratio of the existing structure ($= \delta_{max}/\delta_{yst}$), μ_{dp} is the ductility ratio of the damper for the yield displacement of

the existing frame ($= \delta_{yst}/\delta_{ydp}$), δ_{yst} is the yield displacement of the existing structure, δ_{ydp} is the yield displacement of the damper, C_{yst} is the yield strength of the existing structure expressed in the form of the shear force coefficient ($= Q_{yst}/W$), β is the energy dissipation ratio of the damper, α_c is the ratio of the yield strength of the damper (C_{ydp}) to the strength of the existing structure (C_{yst}) or strength ratio of the damper ($= C_{ydp}/C_{yst}$), and α_k is the ratio of the yield point stiffness of the damper (K_{dp}) to the yield point stiffness of the existing structure (K_{yst}) or stiffness ratio of the damper ($= K_{dp}/K_{yst}$).

In this study, the target seismic performance after seismic retrofitting (E_{R_o}) was set based on Equation (21)—proposed by Jung and Lee [56] after researching the correlations between various seismic acceleration levels and the basic performance index for existing R/C buildings. The target performance ($E_{R_o} = 0.52$) was the level of performance that led to less than moderate seismic damage (life safety) under the aforementioned seismic acceleration of $\alpha = 0.2g(200\ \mathrm{cm/s^2})$.

$$E_{R_o} = 2.7\alpha - 0.02 \tag{21}$$

Here, α is the level of input ground motion divided by gravitational acceleration (g).

Meanwhile, a non-linear static analysis was conducted to calculate the basic performance index of the target building before retrofitting (E_o), i.e., the yield strength (C_y), to determine the seismic reinforcement volume for the building. Figure 34 shows the load–displacement relationship of the existing target R/C building based on the non-linear static analysis.

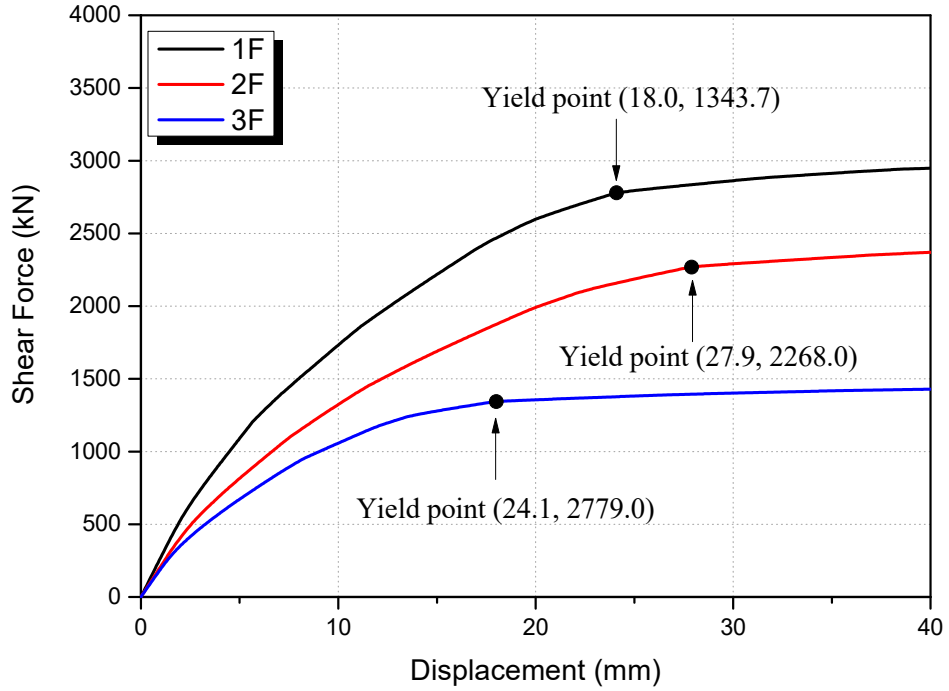

Figure 34. Load–displacement relations based on the non-linear static analysis of non-strengthened control buildings.

The yield strength and displacement in the figure were defined based on Park's definition [57], which is the most realistic definition available for the yield displacement for RC structures. The yield displacement of the equivalent elastoplastic system with a reduced stiffness is the secant stiffness at 75% of the ultimate lateral load of the system. Table 16 shows the yield displacement, strength at the time of yielding (yield strength), and basic performance index of the target building calculated based on the yield strength. The structure and material properties of the LLFD were the same as the results shown in the specimen overview in Section 3 and those applied in the analysis model in Section 5. Based

on these considerations, the required strength and quantity of the LLFD V-bracing system for the target building were finally determined, as listed in Table 17.

Table 16. Basic seismic capacity index (E_o) of non-strengthened control buildings.

Floor	Floor Height [mm]	Floor Weight W [kN]	Yield Displacement δ_y [mm]	Yield Strength V_y [kN]	Failure Mode	Basic Seismic Capacity Index E_o
1	3300	1133.4	24.1	2779.0	Shear failure	0.24
2	3300	7556	27.9	2268.0	Shear failure	0.23
3	3300	3778	18.0	1343.7	Shear failure	0.23

Table 17. Calculated seismic strengthening amount of LLFD V-typed seismic control system.

Floor	Yield Displacement of Damper δ_{ydp} [mm]	Yield Strength of Damper [kN]	Accumulated Deformation Factor β	Targeted Performance E_{Ro}	Required Damper Strength Q_{ydp}	Number of Required Dampers [EA]	Number of Applied Dampers [EA]
1	0.08	125	10	0.52	500.1	4.01	4
2				0.52	418.6	3.36	4
3				0.52	256.1	2.06	2

6.2. Non-Linear Dynamic Analysis Results before and after Seismic Retrofitting

The non-linear dynamic analysis conducted before and after seismic retrofitting based on the non-linear dynamic analysis method presented in Section 6.1 indicated that shear cracks occurred in the columns on the first floor at 2.1 s (3.9 mm) for the non-reinforced building. In addition, a maximum seismic response value of 3584.2 kN was observed, and the building collapsed at 3.3 s (49.1 mm). In the case of the target building retrofitted with the LLFD V-bracing system, fine bending and shear cracks occurred in the columns on the first floor at 2.82 s (3.9 mm); however, no additional maximum response occurred after showing the maximum seismic response at 3.59 s (7.5 mm), resulting in insignificant seismic damage.

Figure 35 shows the load–displacement and time–displacement hysteresis curves for the first floor of the non-reinforced and LLFD-reinforced buildings when subjected to 200 cm/s^2. Table 18 lists the maximum response strength, maximum response displacement, and displacement ratio—important elements for seismic performance assessment—among the analysis results for the LLFD-reinforced building and non-reinforced building subjected to 200 cm/s^2.

According to the above figure and table, compared to the non-reinforced building, the displacement of the LLFD-reinforced building was suppressed by approximately 0.15 times on the first floor, 0.23 times on the second floor, and 0.36 times on the third floor under the input ground motion of 200 cm/s^2, confirming the effectiveness of the seismic retrofitting design and proposed LLFD method.

Meanwhile, as shown in Figures 36 and 37 and Table 19, the LLFD V-bracing system was found to share approximately 67% of the total seismic energy acting on the target R/C school building with non-seismic details as a result of its excellent energy dissipation capacity.

Figures 38 and 39 show the ductility ratio (μ_s) with respect to shear displacement of the columns on each floor of the non-reinforced R/C building and the building retrofitted using the LLFD V-bracing system.

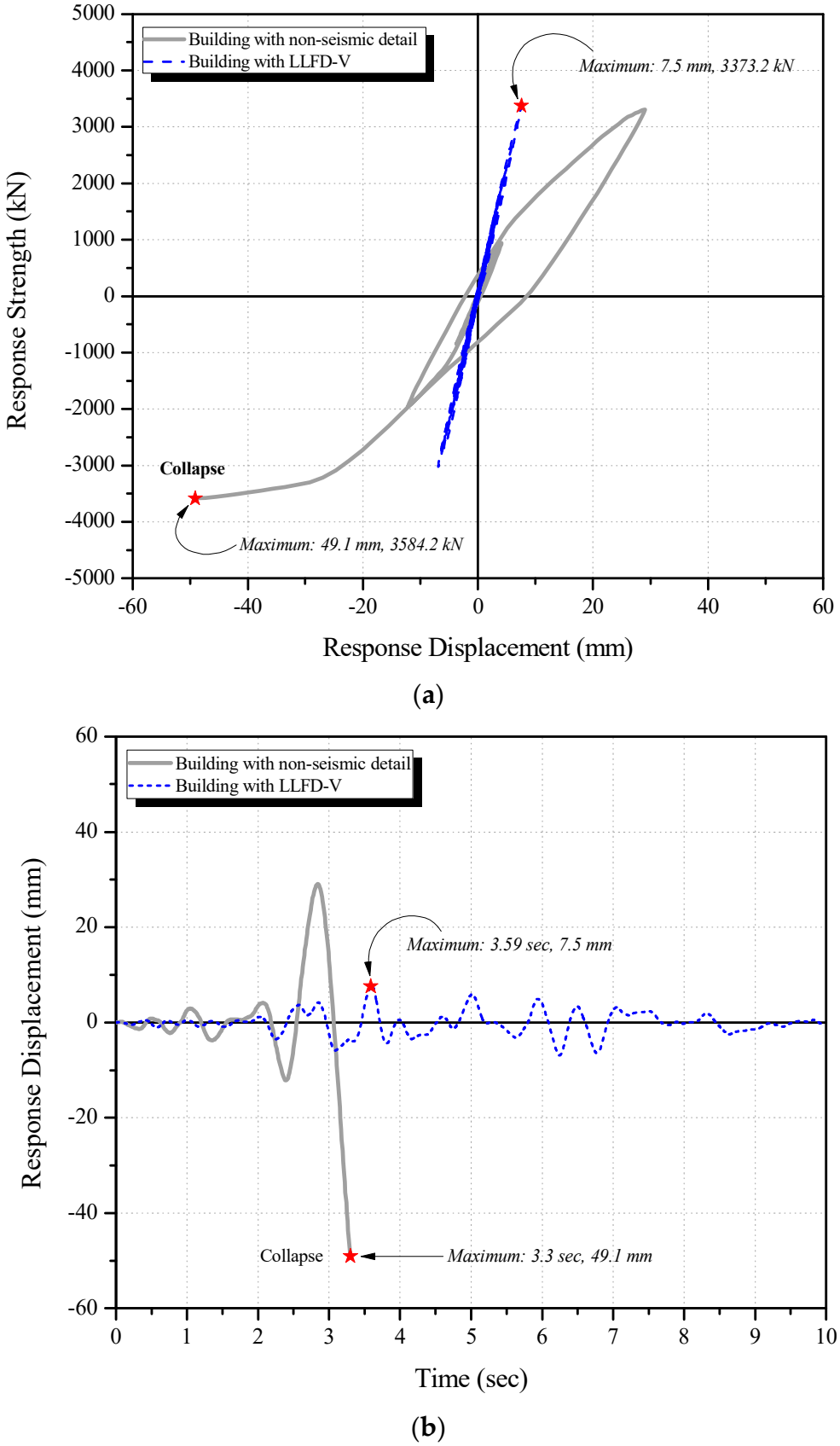

Figure 35. Relationships of analysis results between non-strengthened and LLFD-strengthened buildings (1F): (**a**) Seismic response load-displacement relationship; (**b**) Seismic response time-displacement relationship.

Table 18. Comparison of maximum seismic response and extent of damage before and after seismic strengthening.

Building	Floor	Maximum Response Strength V_{max} [kN]	Maximum Response Displacement and Displacement Ratio δ_{max} [mm]	Failure Mode	Degree of Damage *
Non-strengthened	1	3584.2	49.1	Shear failure	Collapse
	2	2651.9	38.2	Shear failure	Large
	3	1411.3	22.6	Shear crack	Small
NBSD-strengthened	1	3373.2	7.5 [0.15]	Flexural and Shear crack	Light
	2	3200.8	8.9 [0.23]	Flexural and Shear crack	Light
	3	1739.4	8.1 [0.36]	Flexural and Shear crack	Light

* The degree of earthquake-induced damage was evaluated based on JBDPA [48] and Maeda et al. [49].

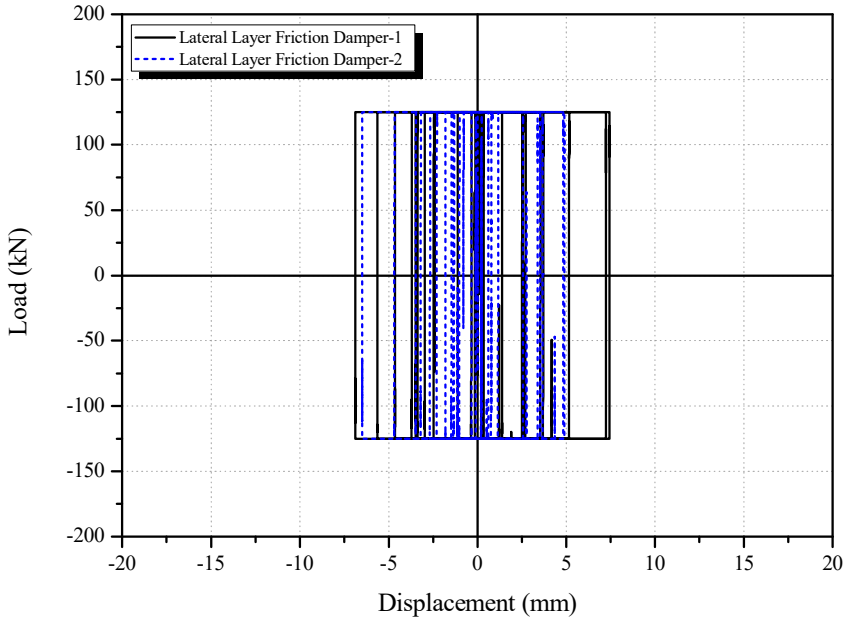

Figure 36. Relationships of seismic response load–displacement for analysis results of LLFD (1F).

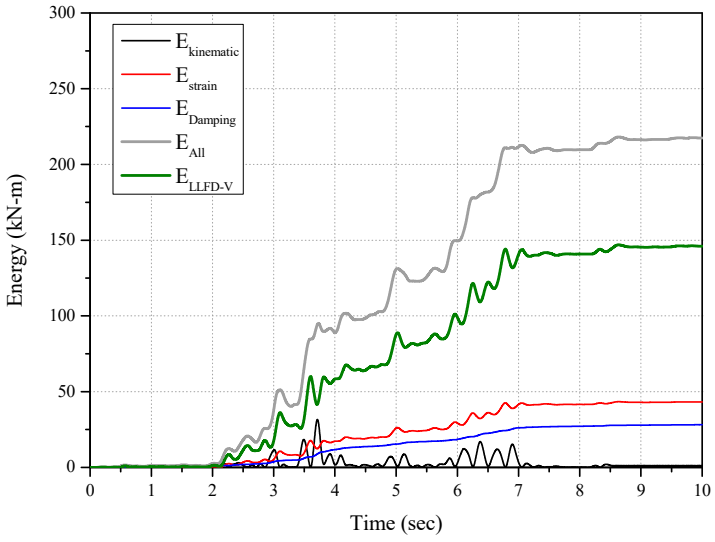

Figure 37. Contribution of the LLFD V-bracing seismic control system to seismic response energy dissipation.

Table 19. Contribution to total energy dissipation capacity by the seismic response of LLFD V-typed seismic control system.

Building	Kinetic Energy E_K [kN·m]	Plastic Deformation Energy E_S [kN·m]	Damping Energy E_D [kN·m]	Total Energy E [kN·m]	Plastic Deformation Energy of LLFD System E_{NBSD} [kN·m]	LLFD System Contribution (%)
NBSD-strengthened	1.06	43.1	28.1	217.4	146.0	67.1

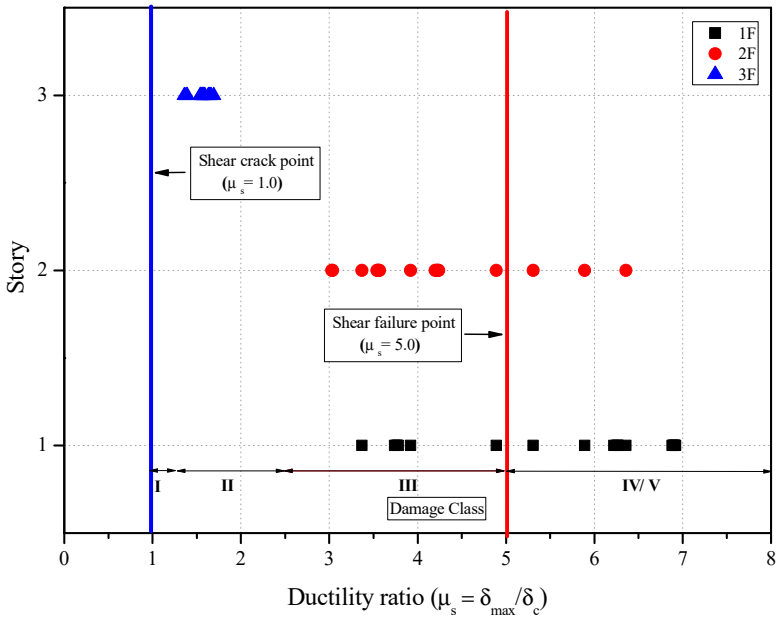

Figure 38. Distribution of ductility ratios of columns with respect to shear displacement of non-reinforced existing buildings based on the non-linear dynamic analysis.

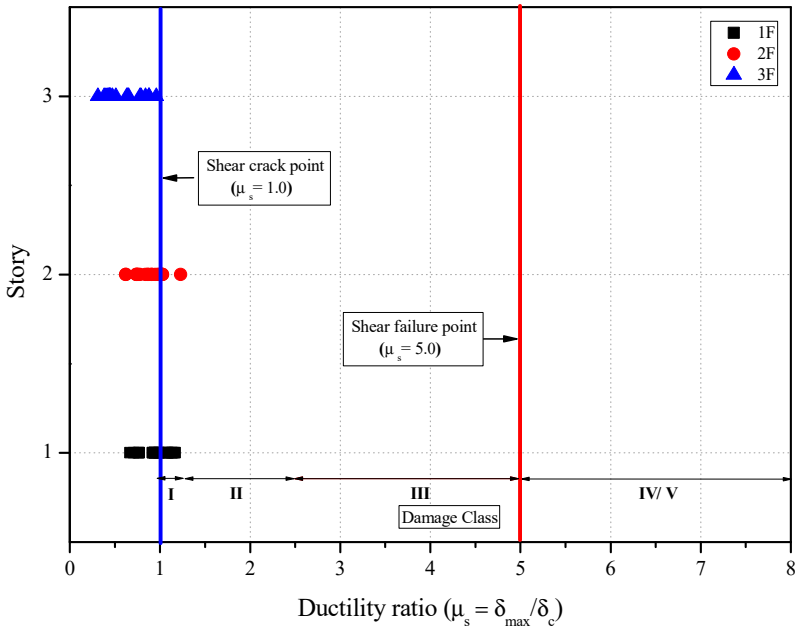

Figure 39. Distribution of ductility ratios of columns with respect to shear displacement of LLFD-strengthened buildings based on the non-linear dynamic analysis.

In the Figures, the ductility ratio with respect to shear displacement was defined as the maximum seismic displacement to the displacement at shear cracking, that is, $\mu_s = \delta_{max}/\delta_c$, as shown in Equation (17), wherein $\mu_s = 1$ represents the time of shear cracking and $\mu_s = 5$ represents the time of shear collapse. In addition, I, II, III, IV, and V in the figures each indicate the damage class of the earthquake designated by JBDPA [48] and Maeda, Nakano, and Lee [49].

As depicted in Figure 38, the non-reinforced R/C building without the seismic details observed shear failure at 15 columns out of 24 columns on the first floor and at 3 columns on the second floor, and it observed shear cracking at all the columns on the third floor. On the contrary, as shown in Figure 39, the LLFD-strengthened building showed shear cracking of $\mu_s = 1.5$ or less or observed no cracking ($\mu_s =$ less than 1) at all the columns of all the floors, indicating that no column exceeded the shear collapse time.

According to JBDPA [48] and Maeda, Nakano, and Lee [49], the earthquake damage level of the non-reinforced R/C building corresponded to collapse, while that of the LLFD-strengthened building corresponded to light damage. The results indicated above showed that the target seismic capacity under the seismic acceleration of 200 cm/s^2 described in Section 6.1, corresponding to moderate earthquake damage (life safety), was satisfied and that the LLFD V-typed system is a new technology that can be commercialized.

7. Conclusions

This study proposed a novel V-bracing system equipped with an LLFD, which could supplement the shortcomings of conventional vibration control systems and is applicable to existing R/C buildings. The material performance and energy dissipation capacity of the LLFD were evaluated using a material test. A pseudo-dynamic test was conducted on two-story frame specimens based on an existing R/C building with non-seismic details to verify the seismic retrofitting effect of applying the LLFD V-bracing system to existing R/C buildings. Based on the pseudo-dynamic test results, restoring force characteristics were proposed for the non-linear dynamic analysis of a building (frame specimen) retrofitted with the LLFD V-bracing system. This non-linear dynamic analysis was conducted based on the proposed restoring force characteristics, with the results obtained compared with the pseudo-dynamic test results. Finally, for evaluating the commercialization potential of the LLFD V-bracing system, a non-linear dynamic analysis was conducted on the existing R/C building with non-seismic details retrofitted with the system. The seismic retrofitting effect was verified by examining the seismic response load and displacement characteristics, energy dissipation capacity, and damper load and displacement response before and after seismic retrofitting. The study results can be summarized as follows.

A cyclic loading test was conducted based on the test method for displacement-dependent vibration control devices presented in KDS 41 [23] to verify the seismic performance of the LLFD V-bracing system. The results suggested that the LLFD specimens exhibited suitable performance as displacement-dependent vibration control devices.

1. When the pseudo-dynamic test was conducted at a DBE scale of 200 cm/s^2, the two-story R/C frame specimen without reinforcement showed shear failure; however, light seismic damage was expected for the frame specimen retrofitted with the LLFD V-bracing system. When a MCE scale of 300 cm/s^2 was assumed, insignificant seismic damage was also expected. Under 400 and 500 cm/s^2—assumed for large earthquakes—moderate seismic damage corresponding to the life safety level was also expected. Compared to the non-reinforced frame that showed the shear failure mode, the failure mode changed from shear failure to bending failure for the specimen retrofitted with the developed LLFD V-bracing system, confirming that the system had an excellent seismic energy dissipation capacity.
2. Compared to the reference specimen, the LLFD method increased the seismic response strength by approximately 1.74 times under the input ground motion of 200 cm/s^2, 2.42 times under 300 cm/s^2, 3.00 times under 400 cm/s^2, and 3.51 times under 500 cm/s^2. The LLFD method also increased the displacement response ratio

by approximately 0.14 times for 200 cm/s^2, 0.23 times for 300 cm/s^2, 0.40 times for 400 cm/s^2, and 0.54 times for 500 cm/s^2 compared to the reference specimen. The seismic response displacement for the same seismic load (200 cm/s^2) was suppressed by approximately 86%, confirming that the proposed LLFD method has an excellent seismic energy absorption capacity.

3. Based on the LLFD member test and pseudo-dynamic test results, the restoring force characteristics of the beams, columns, and reinforcement (LLFD) were proposed for the non-linear dynamic analysis of a two-story frame specimen retrofitted with the LLFD method. Based on the proposed restoring force characteristics, a non-linear dynamic analysis was conducted on the pseudo-dynamic test specimens, with the results obtained compared with the pseudo-dynamic test results. The results were found to be similar, with average differences in the seismic response load and displacement values of less than 10%, indicating that the seismic retrofitting effect of the novel V-bracing system could be effectively evaluated using the non-linear dynamic analysis based on the non-linear analysis model and method constructed in this study.
4. For evaluating the commercialization potential of the LLFD V-bracing system, a non-linear dynamic analysis was conducted on the existing R/C building with non-seismic details retrofitted with the system, with the seismic retrofitting effect before and after seismic retrofitting examined. The R/C building with non-seismic details showed shear failure under a DBE seismic scale of 200 cm/s^2, with insignificant seismic damage anticipated for the R/C building retrofitted with the system because approximately 67% of the total seismic energy acting on the building was shared through the excellent energy dissipation capacity of the LLFD. These results indicated that the developed LLFD V-bracing system is a new seismic retrofitting method that could be commercialized.
5. To commercialize the technology, it is necessary to propose an external joining method that allows the building to be used even during the construction of the LLFD V-bracing system. Therefore, as a recommendation for future research, it is necessary to verify the reliability of the model through detail, experimental verification, and nonlinear dynamic analysis for external coupling applications.

Author Contributions: All authors have contributed to the development of the research and the elaboration of this article. Particularly, B.-G.L. contributed to the methodology and the experimental research, conceptualization; J.-Y.K. contributed to the experimental research and the dynamic analysis; J.-S.J. contributed to the experimental research and the dynamic analysis; and K.-S.L. contributed to the methodology, experimental research, and dynamic analysis, and edited the manuscript. All authors have read and agreed to the published version of the manuscript.

Funding: This paper was supported by a grant (RS-2023-00220751) from the National Research Foundation of Korea (NRF) of the Korean government.

Institutional Review Board Statement: Not applicable.

Informed Consent Statement: Not applicable.

Data Availability Statement: All datasets generated in this study are available from the corresponding author upon reasonable request. The data are not publicly available due to privacy.

Conflicts of Interest: The authors declare no conflict of interest.

References

1. AIK (Architectural Institute of Korea). *Site Inspection and Damage Investigation of Buildings by Earthquakes in Gyoungju and Pohang*; AIK: Seoul, Repblic of Korea, 2018. (In Korean)
2. KMA (Korea Meteorological Administration), Korea. 2023. Available online: https://www.kma.go.kr/eng/index.jsp (accessed on 24 September 2023).
3. Federal Emergency Management Agency (FEMA) 356. *Prestandard and Commentary for Seismic Rehabilitation of Buildings*; Federal Emergency Management Agency (FEMA): Washington, DC, USA, 2000; 500p.

4. Japan Building Disaster Prevention Association (JBDPA). *Guideline for Seismic Strengthening of Existing Reinforced Concrete Buildings*; Japan Building Disaster Prevention Association (JBDPA): Tokyo, Japan, 2017; 450p.
5. Seismic Strengthening Research Group (SSRG). *Seismic Strengthening of RC Buildings*; Ohmsha Press: Tokyo, Japan, 2008; 230p.
6. Pankaj, M.; Singh, S.B. Out-of-plane response of ECC-strengthened masonry walls. *J. Struct. Integr. Maint.* **2020**, *5*, 18–30.
7. Corey, T.G. Multi-performance retrofits to commercial buildings in seismic zones. *J. Struct. Integr. Maint.* **2017**, *2*, 133–142.
8. Alahi, F.N.; Vatandoost, M. Single diagonal precast prestressed concrete bracing for strengthening existing concrete frames. *Int. J. Adv. Struct. Eng.* **2018**, *10*, 339–347. [CrossRef]
9. Cho, C.G.; Cheong, S.H.; Moon, H.J.; Kim, H.Y.; Lee, K.S. Experimental Study on Seismic Capacity of Reinforced Concrete Composite Columns Based on a High-ductile Fiber Cementitious Composite. *Int. J. Concr. Struct. Mater.* **2019**, *13*, 16. [CrossRef]
10. Kurosawa, R.; Sakata, H.; Qu, Z.; Suyama, T. Cyclic loading tests on RC moment frames retrofitted by PC frames with mild press joints through RC slabs for connection. *Eng. Struct.* **2019**, *197*, 109440. [CrossRef]
11. Cao, X.Y.; Feng, D.C.; Wu, G. Seismic performance upgrade of RC frame buildings using precast bolt-connected steel-plate reinforced concrete frame-braces. *Eng. Struct.* **2019**, *195*, 382–399. [CrossRef]
12. Cao, X.Y.; Wu, G.; Ju, J.W.W. Seismic performance improvement of existing RCFs using external PT-PBSPC frame sub-structures: Experimental verification and numerical investigation. *J. Build. Eng.* **2022**, *46*, 103649. [CrossRef]
13. Lee, H.J.; Lee, H.B.; Park, H.G.; Lee, J.K. Cyclic Lateral Load Test for RC Moment Frames Retrofitted with External Steel Frames. *J. Struct. Eng.* **2023**, *149*, 04023028. [CrossRef]
14. Lee, K.S. Experimental Study on Sprayed FRP System for Strengthening Reinforced Concrete Beams. *J. Adv. Concr. Technol.* **2012**, *10*, 219–230. [CrossRef]
15. Lee, K.S.; Lee, B.Y.; Seo, S.Y. A Seismic Strengthening Technique for Reinforced Concrete Columns Using Sprayed FRP. *Polymers* **2016**, *8*, 107. [CrossRef]
16. Ozbakkaloglu, T.; Saatcioglu, M. Tensile behavior of FRP anchors in concrete. *Journal of Composites for Construction* **2009**, *12*, 82–92. [CrossRef]
17. Ju, M.K.; Sim, J.S.; Kwon, H.W.; Lee, K.S. Non-compression cross-bracing system using carbon fiber anchors for seismic strengthening of RC structures. *Mag. Concr. Res.* **2013**, *66*, 159–174. [CrossRef]
18. Belarbi, A.; Acun, B. FRP Systems in Shear Strengthening of Reinforced Concrete Structures. *Procedia Eng.* **2013**, *57*, 2–8. [CrossRef]
19. Lee, K.S. An Experimental Study on Hybrid Noncompression CF Bracing and GF Sheet Wrapping Reinforcement Method to Restore Damaged RC Structures. *Shock. Vib.* **2015**, *2015*, 202751. [CrossRef]
20. *ASCE 7-10*; Minimum Design Loads for Buildings and Other Structures. ASCE American Society of Civil Engineers: Reston, VA, USA, 2010.
21. *ASCE/SEI 7-22*; Minimum Design Loads and Associated Criteria for Buildings and Other Structures. ASCE American Society of Civil Engineers: Reston, VA, USA, 2022.
22. Japan Building Disaster Prevention Association (JBDPA). *Guideline for Seismic Strengthening by Seismic Control and Base Isolation Systems of Existing Reinforced Concrete Buildings*; Japan Building Disaster Prevention Association (JBDPA): Tokyo, Japan, 2010; 129p.
23. *KDS 41*; Korean Design Standard 41. Architectural Institute of Korea: Seoul, Republic of Korea, 2019. (In Korean)
24. Zhang, Y.; Zhu, S. Seismic response control of building structures with superelastic shape memory alloy wire dampers. *J. Eng. Mech.* **2008**, *134*, 240–251. [CrossRef]
25. De Matteis, G.; Formisano, A.; Mazzolani, F.M. An innovative methodology for seismic retrofitting of existing RC buildings by metal shear panels. *Earthq. Eng. Struct. Dyn.* **2009**, *38*, 61–78. [CrossRef]
26. Vemuri. Conducted Research on a Link That Acts as a Sacrificial Fuse by Dissipating Seismic Energy among the Key Components of EBF. 2015. Available online: https://link.springer.com/chapter/10.1007/978-81-322-2190-6_46 (accessed on 1 November 2023).
27. Shi, F.; Ozbulut, O.E.; Zhou, Y. Influence of shape memory alloy brace design parameters on seismic performance of self-centering steel frame buildings. *Struct. Control Health Monit.* **2020**, *27*, e2462. [CrossRef]
28. Yao, Z.; Wang, W.; Zhu, Y. Experimental evaluation and numerical simulation of low-yield-point steel shear panel dampers. *Eng. Struct.* **2021**, *245*, 112860. [CrossRef]
29. Ferraioli, M.; Biagio, L.; Angelo, L.; Frattolillo, C.; de Matteis, G. Seismic retrofit of a steel-reinforced concrete hospital building using continuous energy-dissipative steel columns. *Steel Compos. Struct.* **2023**, *47*, 467–488.
30. Mualla, I.H.; Belev, B. Performance of steel frames with a new friction damper device under earthquake excitation. *Eng. Struct.* **2002**, *24*, 365–371. [CrossRef]
31. Monir, H.S.; Zeynali, K. A modified friction damper for diagonal bracing of structures. *J. Constr. Steel Res.* **2013**, *87*, 17–30. [CrossRef]
32. Ghorbani, H.R.; Rofooei, F.R. A novel double slip loads friction damper to control the seismic response of structures. *Eng. Struct.* **2020**, *225*, 111273. [CrossRef]
33. Veismoradi, S.; Yousef-beik, S.M.M.; Zarnani, P.; Quenneville, P. Development and parametric study of a new self-centering rotational friction damper. *Eng. Struct.* **2021**, *235*, 112097. [CrossRef]
34. Qiu, C.; Liu, J.; Du, X. Cyclic behavior of SMA slip friction damper. *Eng. Struct.* **2022**, *250*, 113407. [CrossRef]

35. Kulak, G.L.; Fisher, J.W.; Struik, J.H. *Guide to Design Criteria for Bolted and Riveted Joints Second Edition*; American Institute of Steel Construction: Chicago, IL, USA, 2014.
36. Takanashi, K.; Udagawa, K.; Tanaka, H. Pseudo-dynamic tests on a 2-storey steel frame by a computer-load test apparatus hybrid system. In Proceedings of the 7th World Conference on Earthquake Engineering, Istanbul, Turkey, 8–13 September 1980; Volume 7, pp. 225–232.
37. Ozcelik, R.; Binici Bari, Ş.; Kurç, O. Pseudo dynamic testing of an RC frame retrofitted with chevron braces. *J. Earthq. Eng.* **2012**, *16*, 515–539. [CrossRef]
38. Di Benedetto, S.; Francavilla, A.B.; Latour, M.; Cavallaro, G.F.; Piluso, V.; Rizzano, G. Pseudo-dynamic testing of a full-scale two-storey steel building with RBS connections. *Eng. Struct.* **2020**, *212*, 110494. [CrossRef]
39. Del Vecchio, C.; Di Ludovico, M.; Verderame, G.M.; Prota, A. Pseudo-dynamic tests on full-scale two storeys RC frames with different infill-to-structure connections. *Eng. Struct.* **2022**, *266*, 114608. [CrossRef]
40. Molitierno, C.; Del Vecchio, C.; Di Ludovico, M.; Prota, A. Pseudodynamic Tests and Numerical Modelling for Damage Analysis of Infilled RC Frames. *J. Earthq. Eng.* **2023**, *287*, 4549–4574. [CrossRef]
41. Tokyo Soki Kenkyujo Company (2020) Tokyo, Japan. Available online: https://www.tml.jp/e/ (accessed on 24 September 2023).
42. MTS. *Pseudodynamic Testing for 793 Controllers*; MTS Systems Corporation: Eden Prairie, MI, USA, 2002.
43. Hilber, H.M.; Hughes, T.J.; Taylor, R.L. Improved numerical dissipation for time integration algorithms in structural dynamics. *Earthq. Eng. Struct. Dyn.* **1977**, *5*, 283–292. [CrossRef]
44. Lee, K.S. Seismic capacity requirements for low-rise reinforced concrete buildings controlled by both shear and flexure. *J. Adv. Concr. Technol.* **2010**, *8*, 75–91. [CrossRef]
45. *KS B 0801*; Test Pieces for Tension Test for Metallic Materials. Korean Industrial Standards: Seoul, Republic of Korea, 2017. (In Korean)
46. *KS B 0802*; Method of Tensile Test for Metallic Materials. Korean Standards Association: Seoul, Republic of Korea, 2018. (In Korean)
47. Lee, K.S.; Wi, J.D.; Kim, Y.I.; Lee, H.H. Seismic safety evaluation of Korean R/C school buildings built in the 1980s. *J. Korean Inst. Struct. Maint. Insp.* **2009**, *13*, 149–159. (In Korean)
48. JBDPA (Japan Building Disaster Prevention Association). *Standard for Damage Level Classification*; JBDPA: Tokyo, Japan, 2015.
49. Maeda, M.; Nakano, Y.; Lee, K.S. Postearthquake damage evaluation for RC buildings based on residual seismic capacity. In Proceedings of the 13th World Conference on Earthquake Engineering, Vancouver, BC, Canada, 1–6 August 2004.
50. Japan Building Disaster Prevention Association (JBDPA). *Japanese Standard for Seismic Evaluation of Existing Reinforced Concrete Buildings*; Japan Building Disaster Prevention Association (JBDPA): Tokyo, Japan, 2017; 550p.
51. AIJ (Architectural Institute of Japan). *Standard for Structural Calculation of Reinforced Concrete Structures*; AIJ: Tokyo, Japan, 2010.
52. Li, K.N. *Canny (Version C11): A 3-Dimensional Nonlinear Dynamic Structural Analysis Computer Program, User Manual*; CANNY Structural Analysis: Vancouver, BC, Canada, 2009.
53. Lee, K.S.; Jung, J.S. A Seismic Capacity of R/C Building Damaged by the 2016 Gyeongju Earthquake Based on the Non-linear Dynamic Analysis. *J. Korea Inst. Struct. Maint. Insp.* **2018**, *22*, 137–146.
54. Matsumoto, Y.; Kitajima, K.; Nakanishi, M.; Adachi, H. A Study on Seismic Retrofit Design of Exiting R/C Buildings by means of Friction Damper. *Proc. Jpn. Concr. Inst.* **1999**, *21*, 391–396. (In Japanese)
55. Yokouchi, H.; Kitajima, K.; Nakanishi, M.; Adachi, H.; Aoyama, H. Experimental Study on Retrofit Effect of an Existing R/C School Building Retrofitted with Energy Dissipation Devices. *J. Struct. Constr. Eng.* **2005**, *70*, 145–152. (In Japanese) [CrossRef] [PubMed]
56. Jung, J.S.; Lee, K.S. A Methodology for Evaluating Seismic Capacity and Seismic Risk Assessment of Reinforced Concrete Buildings in Korea. *J. Asian Archit. Build. Eng.* **2020**, *19*, 103–122. [CrossRef]
57. Park, R. Ductility evaluation form laboratory and analytical testing. In Proceedings of the 9th World Conference on Earthquake Engineering in Japan, Tokyo, Japan, 2–9 August 1988; Volume VIII, pp. 605–616.